

How does non-linear dynamics affect the baryon acoustic oscillation?

Naonori S. Sugiyama^{a,b} and David N. Spergel^b

^aAstronomical Institute, Graduate school of Science, Tohoku University, Sendai 980-8578, Japan

^bDepartment of Astrophysical Sciences, Peyton Hall, Princeton University, NJ 08544, USA

E-mail: nao.s.sugiyama@gmail.com

Abstract.

We study the non-linear behavior of the baryon acoustic oscillation in the power spectrum and the correlation function by decomposing the dark matter perturbations into the short- and long-wavelength modes. The evolution of the dark matter fluctuations can be described as a global coordinate transformation caused by the long-wavelength displacement vector acting on short-wavelength matter perturbation undergoing non-linear growth. Using this feature, we investigate the well known cancellation of the high- k solutions in the standard perturbation theory. While the standard perturbation theory naturally satisfies the cancellation of the high- k solutions, some of the recently proposed improved perturbation theories do not guarantee the cancellation. We show that this cancellation clarifies the success of the standard perturbation theory at the 2-loop order in describing the amplitude of the non-linear power spectrum even at high- k regions.

We propose an extension of the standard 2-loop level perturbation theory model of the non-linear power spectrum that more accurately models the non-linear evolution of the baryon acoustic oscillation than the standard perturbation theory. The model consists of simple and intuitive parts: the non-linear evolution of the smoothed power spectrum without the baryon acoustic oscillations and the non-linear evolution of the baryon acoustic oscillations due to the large-scale velocity of dark matter and due to the gravitational attraction between dark matter particles. Our extended model predicts the smoothing parameter of the baryon acoustic oscillation peak at $z = 0.35$ as $\sim 7.7 \text{ Mpc}/h$ and describes the small non-linear shift in the peak position due to the galaxy random motions.

Keywords: baryon acoustic oscillations, power spectrum

1 Introduction

Large-scale structure surveys are measuring the galaxy power spectrum and the position of the baryon acoustic peak with ever increasing precision [1–10]. In the coming decade, we anticipate that new ground-based surveys such as the Prime Focus Spectrograph and Big BOSS and space-based surveys such as Euclid and WFIRST will make even more accurate measurements of the galaxy power spectrum. Cosmologists will use its shape and the position of the BAO peak to elucidate the nature of dark energy.

These precision measurements demand precision numerical and theoretical work to describe the non-linear evolution of dark matter and the galaxy power spectrum. Many different approaches have been developed over the past decade for understanding this evolution: standard perturbation theory (SPT; [11–19]), Lagrangian resummation theory (LRT; [20, 21]), renormalized perturbation theory (RPT; [22–24]), closure theory [25, 26], multi-point propagator method (the Γ -expansion method; [27–31]), regularized multi-point propagator method (Reg PT; [28, 32, 33]), the Wiener Hermite expansion method [34], as well as other techniques [35–42]. This plethora of techniques has been both stimulating and at times confusing. Why do some methods work, while others are less successful at capturing the non-linear evolution of structure?

In this paper, we explore why the SPT solution succeeds in describing the amplitude of the non-linear power spectrum at high- k regions, focusing the well known cancellation of its solution at the high- k limit. We show that the cancellation is related to the fact that the evolution of the dark matter fluctuations can be described as a global coordinate transformation caused by the long-wavelength displacement vector acting on short-wavelength matter perturbation undergoing non-linear growth. While SPT naturally satisfies the cancellation of the high- k solutions, some of the recently proposed improved perturbation theories, such as RegPT and LRT, do not guarantee the cancellation. Because of this, we confirm that the SPT solution at the 2-loop order still accurately predicts the non-linear matter power spectrum.

We suggest an improvement to the SPT 2-loop solution that more accurately models BAO behavior. This model has two intuitive parts: the smoothed non-linear power spectrum evolution and the non-linear shift of BAO feature. The non-linear evolution of BAO feature is due to two effects: the primary effect is due to the large-scale velocity field and the secondary effect is due to the gravitational correlation effect between dark matter particles.

The N -body simulation results used in this paper were presented in [43]. These results and initial conditions at $z_{\text{ini}} = 99$ were created by the public N -body codes *GADGET2* and *2LPT* code, respectively [44, 45]. These N -body simulations contain 2048^3 particles and were computed by combining the results with different box sizes $2048h^{-1}$ Mpc and $4096 h^{-1}$ Mpc, called *L11-N11* and *L12-N11*. The cosmological parameters we used were presented by the *Wilkinson Microwave Anisotropy Probe (WMAP)* five year release [46] ($\Omega_m = 0.279$, $\Omega_\Lambda = 0.721$, $\Omega_b = 0.046$, $h = 0.701$, $n_s = 0.96$ and $\sigma_8 = 0.817$). We used the program which is available on Taruya’s homepage to compute the predicted power spectra ¹.

This paper is organized as follows. In sections 2 and 3, we perform the decomposition of the matter perturbation into the long- and short-wavelength terms in the Eulerian and Lagrangian descriptions, respectively. In section 4, we show the relation between the long- and short-wavelength decomposition and the well known cancellation in the SPT solution at the high- k limit. Section 5 presents the non-linear power spectrum model including the more accurate information on BAO than SPT. In section 6, we compute the correlation function using our non-linear power spectrum model and investigate the non-linear shift of BAO. In section 7, we summarize and discuss our result.

¹ <http://www-utap.phys.s.u-tokyo.ac.jp/~ataruya/>

2 Standard Perturbation Theory (SPT)

2.1 Review of SPT

In SPT, the matter density field and the divergence of the velocity density field, $\theta \equiv \nabla \cdot \mathbf{v}$, is expanded out in a perturbation series in the linear growth function, D , in Fourier space: [11]

$$\delta(z, \mathbf{k}) = \sum_{n=1}^{\infty} D^n \delta_n(\mathbf{k}), \quad \theta(z, \mathbf{k}) = -aHf \sum_{n=1}^{\infty} D^n \theta_n(\mathbf{k}), \quad (2.1)$$

where z , H , and a , are the redshift, the Hubble parameter and the scale factor. The velocity field scales as $f = d \ln D / d \ln a \simeq \Omega^{0.5}$.

The n th-order perturbations are given by

$$\begin{aligned} \delta_n(\mathbf{k}) &= \int \frac{d^3 p_1}{(2\pi)^3} \cdots \frac{d^3 p_n}{(2\pi)^3} (2\pi)^3 \delta_{\mathbf{D}}(\mathbf{k} - \mathbf{p}_{[1,n]}) F_n([\mathbf{p}_1, \mathbf{p}_n]) \delta_{\text{lin}}(\mathbf{p}_1) \cdots \delta_{\text{lin}}(\mathbf{p}_n), \\ \theta_n(\mathbf{k}) &= \int \frac{d^3 p_1}{(2\pi)^3} \cdots \frac{d^3 p_n}{(2\pi)^3} (2\pi)^3 \delta_{\mathbf{D}}(\mathbf{k} - \mathbf{p}_{[1,n]}) G_n([\mathbf{p}_1, \mathbf{p}_n]) \delta_{\text{lin}}(\mathbf{p}_1) \cdots \delta_{\text{lin}}(\mathbf{p}_n), \end{aligned} \quad (2.2)$$

where $F_n(\mathbf{p}_1, \dots, \mathbf{p}_n) \equiv F_n([\mathbf{p}_1, \mathbf{p}_n])$, $\mathbf{p}_{[1,n]} \equiv \mathbf{p}_1 + \cdots + \mathbf{p}_n$, and $\delta_1(\mathbf{k}) \equiv \delta_{\text{lin}}(\mathbf{k})$.

Under the condition that the amplitudes of m Fourier modes $\mathbf{p}_1, \dots, \mathbf{p}_m$ in F_n and G_n are much smaller than those of the others,

$$|\mathbf{p}_{m+1}|, \dots, |\mathbf{p}_n| \gg |\mathbf{p}_1|, \dots, |\mathbf{p}_m| \rightarrow 0, \quad (2.3)$$

the n th-order kernel functions are represented by the lower m th-order ones than n [18]:

$$\begin{aligned} F_n(\mathbf{p}_1, \mathbf{p}_n) \Big|_{p_1, \dots, p_m \rightarrow 0} &\rightarrow \frac{(n-m)!}{n!} \left(\frac{\mathbf{p}_{[m+1,n]} \cdot \mathbf{p}_1}{p_1^2} \right) \cdots \left(\frac{\mathbf{p}_{[m+1,n]} \cdot \mathbf{p}_m}{p_m^2} \right) F_{n-m}([\mathbf{p}_{m+1}, \mathbf{p}_n]), \\ G_n(\mathbf{p}_1, \mathbf{p}_n) \Big|_{p_1, \dots, p_m \rightarrow 0} &\rightarrow \frac{(n-m)!}{n!} \left(\frac{\mathbf{p}_{[m+1,n]} \cdot \mathbf{p}_1}{p_1^2} \right) \cdots \left(\frac{\mathbf{p}_{[m+1,n]} \cdot \mathbf{p}_m}{p_m^2} \right) G_{n-m}([\mathbf{p}_{m+1}, \mathbf{p}_n]). \end{aligned} \quad (2.4)$$

2.2 Decomposition into the long- and short-wavelength modes in SPT

What is the physical meaning of the expressions of the kernel functions in eq. (2.4)? To study this, we shall decompose the linear matter density perturbation into the long- and short-wavelength modes as

$$\delta_{\text{lin}}(\mathbf{k}) = \delta_{\text{lin}}^{(\text{L})}(\mathbf{k}) + \delta_{\text{lin}}^{(\text{S})}(\mathbf{k}), \quad (2.5)$$

where the linear long-wavelength mode is defined as $\delta_{\text{lin}}(\mathbf{k})|_{\mathbf{k} \rightarrow 0} \equiv \delta_{\text{lin}}^{(\text{L})}(\mathbf{k})$. We substitute eq. (2.5) into the solution in SPT [eqs. (2.1) and (2.2)]:

$$\begin{aligned} \delta(z, \mathbf{k}) &= \sum_{n=1}^{\infty} D^n \int \frac{d^3 p_1}{(2\pi)^3} \cdots \int \frac{d^3 p_n}{(2\pi)^3} (2\pi)^3 \delta_{\mathbf{D}}(\mathbf{k} - \mathbf{p}_{[1,n]}) F_n([\mathbf{p}_1, \mathbf{p}_n]) \Big|_{p_1, \dots, p_n \rightarrow 0} \delta_{\text{lin}}^{(\text{L})}(\mathbf{p}_1) \cdots \delta_{\text{lin}}^{(\text{L})}(\mathbf{p}_n) \\ &+ \sum_{n=1}^{\infty} D^n \sum_{m=0}^{n-1} \frac{n!}{m!(n-m)!} \int \frac{d^3 p_1}{(2\pi)^3} \cdots \int \frac{d^3 p_n}{(2\pi)^3} (2\pi)^3 \delta_{\mathbf{D}}(\mathbf{k} - \mathbf{p}_{[1,n]}) F_n([\mathbf{p}_1, \mathbf{p}_n]) \Big|_{p_1, \dots, p_m \rightarrow 0} \\ &\quad \times \delta_{\text{lin}}^{(\text{L})}(\mathbf{p}_1) \cdots \delta_{\text{lin}}^{(\text{L})}(\mathbf{p}_m) \delta_{\text{lin}}^{(\text{S})}(\mathbf{p}_{m+1}) \cdots \delta_{\text{lin}}^{(\text{S})}(\mathbf{p}_n). \end{aligned} \quad (2.6)$$

The first term in the right-hand side is the contribution from the long-wavelength modes and the second term is the combination of the long- and short-wavelength modes. The conditions of $p_1, \dots, p_n \rightarrow 0$ and $p_1, \dots, p_m \rightarrow 0$ are imposed on the kernel functions because of the long-wavelength modes of the linear matter perturbations. The first term becomes zero for $n \geq 2$ due to $F_n([\mathbf{p}_1, \mathbf{p}_n])|_{p_1, \dots, p_n \rightarrow 0} (n \geq$

2) $\rightarrow 0$. This implies that no non-linear effect contributes to the evolution of dark matter in the large-scale limit, an inevitable consequence of mass and momentum conservation. Since we are interested in the small scales where the non-linear effects contribute to the evolution of the matter perturbation, from now on we ignore the linear matter perturbation in the first term. Using eq. (2.4), we find

$$\begin{aligned}
\delta(z, \mathbf{k}) &= \sum_{n=1}^{\infty} D^n \sum_{m=0}^{n-1} \frac{1}{m!} \prod_{i=0}^m \left[\int \frac{d^3 p_i}{(2\pi)^3} \left(\frac{\mathbf{p}_{[m+1, n]} \cdot \mathbf{p}_i}{p_i^2} \right) \delta_{\text{lin}}^{(L)}(\mathbf{p}_i) \right] \\
&\quad \times \int \frac{d^3 p_{m+1}}{(2\pi)^3} \cdots \int \frac{d^3 p_n}{(2\pi)^3} (2\pi)^3 \delta_{\text{D}}(\mathbf{k} - \mathbf{p}_{[1, n]}) F_{n-m}([\mathbf{p}_{m+1}, \mathbf{p}_n]) \delta_{\text{lin}}^{(S)}(\mathbf{p}_{m+1}) \cdots \delta_{\text{lin}}^{(S)}(\mathbf{p}_n) \\
&= \sum_{n=m=1}^{\infty} D^{n-m} \int d^3 x e^{-i\mathbf{k} \cdot \mathbf{x}} \sum_{m=0}^{\infty} \frac{1}{m!} \left[-i\mathbf{p}_{[m+1, n]} \cdot \int \frac{d^3 p}{(2\pi)^3} e^{i\mathbf{p} \cdot \mathbf{x}} D\mathbf{\Psi}_{\text{lin}}^{(L)}(\mathbf{p}) \right]^m \\
&\quad \times \int \frac{d^3 p_{m+1}}{(2\pi)^3} \cdots \int \frac{d^3 p_n}{(2\pi)^3} e^{i\mathbf{p}_{[m+1, n]} \cdot \mathbf{x}} F_{n-m}([\mathbf{p}_{m+1}, \mathbf{p}_n]) \delta_{\text{lin}}^{(S)}(\mathbf{p}_{m+1}) \cdots \delta_{\text{lin}}^{(S)}(\mathbf{p}_n), \quad (2.7)
\end{aligned}$$

where in the second equality we used the summation relation of $\sum_{n=1}^{\infty} \sum_{m=0}^{n-1} = \sum_{n-m=1}^{\infty} \sum_{m=0}^{\infty}$ and $(2\pi)^3 \delta_{\text{D}}(\mathbf{k} - \mathbf{p}_{[1, n]}) = \int d^3 x e^{-i(\mathbf{k} - \mathbf{p}_{[1, n]}) \cdot \mathbf{x}}$, and defined the linear displacement vector as

$$\frac{i\mathbf{p}}{p^2} \delta_{\text{lin}}(\mathbf{p}) = \frac{\mathbf{v}_{\text{lin}}(\mathbf{p})}{DaH} \equiv \mathbf{\Psi}_{\text{lin}}(\mathbf{p}). \quad (2.8)$$

Fourier transforming the displacement vector leads to

$$\delta(z, \mathbf{k}) = \sum_{n=1}^{\infty} D^n \int d^3 x e^{-i\mathbf{k} \cdot \mathbf{x}} \int \frac{d^3 p_1}{(2\pi)^3} \cdots \int \frac{d^3 p_n}{(2\pi)^3} e^{i\mathbf{p}_{[1, n]} \cdot (\mathbf{x} - D\mathbf{\Psi}_{\text{lin}}^{(L)}(\mathbf{x}))} F_n([\mathbf{p}_1, \mathbf{p}_n]) \delta_{\text{lin}}^{(S)}(\mathbf{p}_1) \cdots \delta_{\text{lin}}^{(S)}(\mathbf{p}_n). \quad (2.9)$$

In the real space, this expression becomes

$$\delta(z, \mathbf{x}) = \delta^{(S)}(z, \mathbf{x} - D\mathbf{\Psi}_{\text{lin}}^{(L)}(\mathbf{x})), \quad (2.10)$$

where the short-wavelength matter perturbation in the real space is defined as

$$\delta^{(S)}(z, \mathbf{x}) \equiv \sum_{n=1}^{\infty} D^n \int \frac{d^3 p_1}{(2\pi)^3} \cdots \int \frac{d^3 p_n}{(2\pi)^3} e^{i\mathbf{p}_{[1, n]} \cdot \mathbf{x}} F_n([\mathbf{p}_1, \mathbf{p}_n]) \delta_{\text{lin}}^{(S)}(\mathbf{p}_1) \cdots \delta_{\text{lin}}^{(S)}(\mathbf{p}_n). \quad (2.11)$$

For the extreme case where the long-wavelength displacement vector behaves as a uniform displacement, $\mathbf{\Psi}_{\text{lin}}^{(L)}(\mathbf{p}) \rightarrow (2\pi)^3 \delta_{\text{D}}(\mathbf{p}) \bar{\mathbf{\Psi}}_{\text{lin}}^{(L)}$ where $\bar{\mathbf{\Psi}}_{\text{lin}}^{(L)}$ is constant, we obtain the following simple expressions in the Fourier and real spaces, respectively:

$$\begin{aligned}
\delta(z, \mathbf{k}) &= e^{-i\mathbf{k} \cdot D\bar{\mathbf{\Psi}}_{\text{lin}}^{(L)}} \delta^{(S)}(z, \mathbf{k}), \\
\delta(z, \mathbf{x}) &= \delta^{(S)}(z, \mathbf{x} - D\bar{\mathbf{\Psi}}_{\text{lin}}^{(L)}), \quad (2.12)
\end{aligned}$$

where the short-wavelength matter perturbation in the Fourier space is defined as

$$\delta^{(S)}(z, \mathbf{k}) \equiv \sum_{n=1}^{\infty} D^n \int \frac{d^3 p_1}{(2\pi)^3} \cdots \int \frac{d^3 p_n}{(2\pi)^3} (2\pi)^3 \delta_{\text{D}}(\mathbf{k} - \mathbf{p}_{[1, n]}) F_n([\mathbf{p}_1, \mathbf{p}_n]) \delta_{\text{lin}}^{(S)}(\mathbf{p}_1) \cdots \delta_{\text{lin}}^{(S)}(\mathbf{p}_n). \quad (2.13)$$

The same analysis for θ leads to

$$\begin{aligned}
\theta(z, \mathbf{k}) &= e^{-i\mathbf{k} \cdot D\bar{\mathbf{\Psi}}_{\text{lin}}^{(L)}} \theta^{(S)}(z, \mathbf{k}), \\
\theta(z, \mathbf{x}) &= \theta^{(S)}(z, \mathbf{x} - D\bar{\mathbf{\Psi}}_{\text{lin}}^{(L)}), \quad (2.14)
\end{aligned}$$

with

$$\theta^{(S)}(z, \mathbf{k}) \equiv -aHf \sum_{n=1}^{\infty} D^n \int \frac{d^3 p_1}{(2\pi)^3} \cdots \int \frac{d^3 p_n}{(2\pi)^3} (2\pi)^3 \delta_D(\mathbf{k} - \mathbf{p}_{[1,n]}) G_n([\mathbf{p}_1, \mathbf{p}_n]) \delta_{\text{lin}}^{(S)}(\mathbf{p}_1) \cdots \delta_{\text{lin}}^{(S)}(\mathbf{p}_n). \quad (2.15)$$

These equations describe our basic picture of representing the matter density perturbation and the velocity divergence of dark matter in terms of a coordinate transformation due to the long-wavelength displacement vector acting on the short wavelength modes. In particular, the extreme long-wavelength mode of the displacement vector $\bar{\Psi}_{\text{lin}}^{(L)}$ globally changes the spatial coordinates throughout the universe without contributing to the non-linear evolution of the matter perturbations. This fact implies that we need only consider the non-linear contributions from the short-wavelength modes $\delta_n^{(S)}$ in computing the non-linear evolution of dark matter.

3 Lagrangian Perturbation Theory

Our decomposition of the matter perturbation into the long- and short- wavelength modes [eq. (2.12)] easily generalizes to the Lagrangian description.

3.1 Review of LPT

In the Lagrangian description, the spatial coordinates are transformed as

$$\mathbf{x} \equiv \mathbf{q} + \Psi(z, \mathbf{q}), \quad (3.1)$$

where Ψ is the displacement vector of dark matter. Conservation of mass implies that the density perturbation can be described as a function of the displacement vector:

$$\begin{aligned} \delta(z, \mathbf{k}) &= \int d^3 q e^{-i\mathbf{k}\cdot\mathbf{q}} \left(e^{-i\mathbf{k}\cdot\Psi(z, \mathbf{q})} - 1 \right) \\ &= \sum_{n=1}^{\infty} \frac{(-i)^n}{n!} \int \frac{d^3 k_1}{(2\pi)^3} \cdots \frac{d^3 k_n}{(2\pi)^3} (2\pi)^3 \delta_D(\mathbf{k} - \mathbf{k}_{[1,n]}) [\mathbf{k} \cdot \Psi(z, \mathbf{k}_1)] \cdots [\mathbf{k} \cdot \Psi(z, \mathbf{k}_n)]. \end{aligned} \quad (3.2)$$

The displacement vector is perturbatively expanded as (see also appendix B)

$$\Psi(z, \mathbf{k}) = \sum_{n=1}^{\infty} D^n \Psi_n(\mathbf{k}), \quad (3.3)$$

where

$$\Psi_n(\mathbf{k}) = \frac{i}{n!} \int \frac{d^3 p_1}{(2\pi)^3} \cdots \frac{d^3 p_n}{(2\pi)^3} (2\pi)^3 \delta_D(\mathbf{k} - \mathbf{p}_{[1,n]}) \mathbf{L}_n(\mathbf{p}_1, \dots, \mathbf{p}_n) \delta_{\text{lin}}(\mathbf{p}_1) \cdots \delta_{\text{lin}}(\mathbf{p}_n). \quad (3.4)$$

3.2 Decomposition into the long- and short-wavelength modes in LPT

Now, we decompose the displacement vector into the long- and short-wavelength modes as

$$\Psi(z, \mathbf{q}) = \bar{\Psi}^{(L)}(z) + \Psi^{(S)}(z, \mathbf{q}). \quad (3.5)$$

The long-wavelength displacement vector is defined as $\bar{\Psi}^{(L)}(z) \equiv \Psi(z, \mathbf{q} = 0)$ whose Fourier-transformation is $(2\pi)^3 \delta_D(\mathbf{k}) \bar{\Psi}^{(L)}(z)$. This decomposition allow us to express the matter perturbation as

$$\begin{aligned} \delta(z, \mathbf{k}) &= \int d^3 q e^{-i\mathbf{k}\cdot\mathbf{q}} \left(e^{-i\mathbf{k}\cdot\bar{\Psi}^{(L)}(z)} - 1 \right) + \int d^3 q e^{-i\mathbf{k}\cdot\mathbf{q}} e^{-i\mathbf{k}\cdot\bar{\Psi}^{(L)}(z)} \left(e^{-i\mathbf{k}\cdot\Psi^{(S)}(z, \mathbf{q})} - 1 \right) \\ &= (2\pi)^3 \delta_D(\mathbf{k}) \left(e^{-i\mathbf{k}\cdot\bar{\Psi}^{(L)}(z)} - 1 \right) + \int d^3 q e^{-i\mathbf{k}\cdot\mathbf{q}} e^{-i\mathbf{k}\cdot\bar{\Psi}^{(L)}(z)} \left(e^{-i\mathbf{k}\cdot\Psi^{(S)}(z, \mathbf{q})} - 1 \right) \\ &= e^{-i\mathbf{k}\cdot\bar{\Psi}^{(L)}(z)} \delta^{(S)}(z, \mathbf{k}), \end{aligned} \quad (3.6)$$

where the first term in the second line becomes zero, and in the third line the short-wavelength matter perturbation is defined as

$$\delta^{(S)}(z, \mathbf{k}) \equiv \int d^3q e^{-i\mathbf{k}\cdot\mathbf{q}} \left(e^{-i\mathbf{k}\cdot\bar{\Psi}^{(S)}(z, \mathbf{q})} - 1 \right). \quad (3.7)$$

In the real space, we have

$$\begin{aligned} \delta(z, \mathbf{x}) &= \delta^{(S)}(z, \mathbf{x} - \bar{\Psi}^{(L)}(z)) \\ &= \delta^{(S)}(z, \mathbf{q} + \Psi^{(S)}(z, \mathbf{q})). \end{aligned} \quad (3.8)$$

This is the first main result of this paper. This result includes the non-linear long-wavelength displacement vector and is clearly a generalized version of eq. (2.12). Note that we do not need any dynamics to derive this expression as long as the matter perturbation is represented by eq. (3.2) which results from the law of the conservation of mass.

4 Power spectrum

Interestingly, the expression for the matter perturbation in eq. (3.6) naturally explains the high- k solutions in SPT. The definitions of the correlation terms at 1- and 2-loop level in SPT are summarized in appendix A.

4.1 Cancellation of high- k solutions in SPT

The high- k solutions in SPT at the 1-loop order is given by

$$\begin{aligned} P_{22, \text{high-}k}(k) &= 2 \times 2 \int \frac{d^3k_1}{(2\pi)^3} \int \frac{d^3k_2}{(2\pi)^3} (2\pi)^3 \delta_D(\mathbf{k} - \mathbf{k}_1 - \mathbf{k}_2) \left[F_2(\mathbf{k}_1, \mathbf{k}_2) \Big|_{\mathbf{k}_1 \rightarrow 0} \right]^2 |P_{\text{lin}}(k_1) P_{\text{lin}}(k_2), \\ &\rightarrow 2 \times 2 \int \frac{d^3k_1}{(2\pi)^3} \int \frac{d^3k_2}{(2\pi)^3} (2\pi)^3 \delta_D(\mathbf{k} - \mathbf{k}_2) \left[\frac{1}{2!} \frac{\mathbf{k}_1 \cdot \mathbf{k}_2}{k_1^2} \right]^2 P_{\text{lin}}(k_1) P_{\text{lin}}(k_2), \\ &= \left(\frac{k^2 \sigma_{v, \text{lin}}^2}{2} \right) P_{\text{lin}}(k), \\ P_{13, \text{high-}k}(k) &= 6 P_{\text{lin}}(k) \int \frac{d^3p}{(2\pi)^3} F_3(\mathbf{k}, \mathbf{p}, -\mathbf{p}) \Big|_{\mathbf{p} \rightarrow 0} P_{\text{lin}}(p), \\ &\rightarrow 6 P_{\text{lin}}(k) \int \frac{d^3p}{(2\pi)^3} \left[-\frac{1}{3!} \left(\frac{\mathbf{k} \cdot \mathbf{p}}{p^2} \right)^2 \right] P_{\text{lin}}(p), \\ &= - \left(\frac{k^2 \sigma_{v, \text{lin}}^2}{2} \right) P_{\text{lin}}(k), \end{aligned} \quad (4.1)$$

where we used Eq. (2.4) and

$$\sigma_{v, \text{lin}}^2 = \frac{1}{3\pi^2} \int dp P_{\text{lin}}(p). \quad (4.2)$$

These high- k solutions are also obtained using the decomposition of the short- and long wavelength parts in Eq. (3.6). From eq. (3.6), the second- and third-order matter perturbations in SPT are described as

$$\begin{aligned} \delta_2(\mathbf{k}) &= \delta_2^{(S)}(\mathbf{k}) + \left(-i\mathbf{k} \cdot \bar{\Psi}_{\text{lin}}^{(L)} \right) \delta_{\text{lin}}^{(S)}(\mathbf{k}), \\ \delta_3(\mathbf{k}) &= \delta_3^{(S)}(\mathbf{k}) + \left(-i\mathbf{k} \cdot \bar{\Psi}_{\text{lin}}^{(L)} \right) \delta_2^{(S)}(\mathbf{k}) + \left(-i\mathbf{k} \cdot \bar{\Psi}_2^{(L)} \right) \delta_{\text{lin}}^{(S)}(\mathbf{k}) + \frac{1}{2} \left(-i\mathbf{k} \cdot \bar{\Psi}_{\text{lin}}^{(L)} \right)^2 \delta_{\text{lin}}^{(S)}(\mathbf{k}). \end{aligned} \quad (4.3)$$

Here, the high- k solutions come from the terms including the decorrelation of the short- and long-wavelength parts:

$$\begin{aligned}
\langle \delta_2(\mathbf{k})\delta_2(\mathbf{k}') \rangle|_{\text{high-}k} &= \left\langle \left(-i\mathbf{k} \cdot \bar{\Psi}_{\text{lin}}^{(L)} \right) \left(-i\mathbf{k}' \cdot \bar{\Psi}_{\text{lin}}^{(L)} \right) \right\rangle \langle \delta_{\text{lin}}^{(S)}(\mathbf{k})\delta_{\text{lin}}^{(S)}(\mathbf{k}') \rangle \\
&= (2\pi)^3 \delta_D(\mathbf{k} + \mathbf{k}') \left[\left(\frac{k^2 \sigma_{v,\text{lin}}^2}{2} \right) P_{\text{lin}}(k) \right], \\
2\langle \delta_3(\mathbf{k})\delta_{\text{lin}}(\mathbf{k}') \rangle|_{\text{high-}k} &= 2 \left\langle \frac{\left(-i\mathbf{k} \cdot \bar{\Psi}_{\text{lin}}^{(L)} \right)^2}{2!} \right\rangle \langle \delta_{\text{lin}}^{(S)}(\mathbf{k})\delta_{\text{lin}}^{(S)}(\mathbf{k}') \rangle \\
&= (2\pi)^3 \delta_D(\mathbf{k} + \mathbf{k}') \left[- \left(\frac{k^2 \sigma_{v,\text{lin}}^2}{2} \right) P_{\text{lin}}(k) \right], \tag{4.4}
\end{aligned}$$

where since we are interested in the small scale regions where the non-linear effects cannot be ignored, we can regard that the linear power spectrum is obtained by $\delta_{\text{lin}}^{(S)}$.

Similarly to the derivation used in eq. (4.4), the high- k solutions at the 2-loop order in SPT [eq. (A.3)] are given by

$$\begin{aligned}
P_{33a,\text{high-}k}(k) &= -\frac{1}{2} \left(\frac{k^2 \sigma_{v,\text{lin}}^2}{2} \right) P_{13}(k) - \frac{1}{4} \left(\frac{k^2 \sigma_{v,\text{lin}}^2}{2} \right)^2 P_{\text{lin}}(k), \\
P_{33b,\text{high-}k}(k) &= \left(\frac{k^2 \sigma_{v,\text{lin}}^2}{2} \right) P_{22}(k) - \frac{1}{2} \left(\frac{k^2 \sigma_{v,\text{lin}}^2}{2} \right)^2 P_{\text{lin}}(k) + \left(\frac{k^2 \sigma_{v,22}^2}{2} \right) P_{\text{lin}}(k), \\
P_{24,\text{high-}k}(k) &= - \left(\frac{k^2 \sigma_{v,\text{lin}}^2}{2} \right) P_{22}(k) + \left(\frac{k^2 \sigma_{v,\text{lin}}^2}{2} \right) P_{13}(k) + \left(\frac{k^2 \sigma_{v,\text{lin}}^2}{2} \right)^2 P_{\text{lin}}(k) + \left(\frac{k^2 \sigma_{v,13}^2}{2} \right) P_{\text{lin}}(k), \\
P_{15,\text{high-}k}(k) &= -\frac{1}{2} \left(\frac{k^2 \sigma_{v,\text{lin}}^2}{2} \right) P_{13}(k) - \frac{1}{4} \left(\frac{k^2 \sigma_{v,\text{lin}}^2}{2} \right)^2 P_{\text{lin}}(k) - \left(\frac{k^2 \sigma_{v,1\text{-loop}}^2}{2} \right) P_{\text{lin}}(k), \tag{4.5}
\end{aligned}$$

where

$$\begin{aligned}
\sigma_{v,22}^2 &\equiv \frac{3}{392 \cdot 32\pi^4} \int \frac{dp_1}{p_1^3} \frac{dp_2}{p_2^3} K(p_1, p_2) P_{\text{lin}}(p_1) P_{\text{lin}}(p_2), \\
\sigma_{v,13}^2 &\equiv \frac{5}{126 \cdot 32\pi^4} \int \frac{dp_1}{p_1^3} \frac{dp_2}{p_2^3} K(p_1, p_2) P_{\text{lin}}(p_1) P_{\text{lin}}(p_2), \\
\sigma_{v,1\text{-loop}}^2 &\equiv \sigma_{v,22}^2 + \sigma_{v,13}^2, \\
&= \frac{167}{3528 \cdot 32\pi^4} \int \frac{dp_1}{p_1^3} \frac{dp_2}{p_2^3} K(p_1, p_2) P_{\text{lin}}(p_1) P_{\text{lin}}(p_2), \tag{4.6}
\end{aligned}$$

with

$$K(p_1, p_2) = (p_1^2 - p_2^2)^4 \ln \left(\frac{(p_1 + p_2)^2}{(p_1 - p_2)^2} \right) - \frac{4}{3} p_1 p_2 (3p_1^6 - 11p_2^2 p_1^4 - 11p_1^2 p_2^4 + 3p_2^6). \tag{4.7}$$

In [21], the expressions of $\sigma_{v,22}^2$ and $\sigma_{v,13}^2$ are represented as $\sigma_{v,22}^2 = \mathcal{A}_{22}/(3\pi^2)$ and $\sigma_{v,13}^2 = 2\mathcal{A}_{13}/(3\pi^2)$, respectively (for details see appendix B). However, the expression of the 1-loop velocity dispersion $\sigma_{v,1\text{-loop}}^2$ in eq. (4.6) is different from eq. (41) in [47] which is shown using the eikonal approximation. Using the expression of the kernel functions in eq. (2.4), we obtain the same expressions as eq. (4.5) except for lack of the terms including $\sigma_{v,13}^2$ and $\sigma_{v,22}^2$ (see [18]). This is the result that the expression in eq. (3.6) is more general than that in eq. (2.12).

Clearly, we find the cancellation of the high- k solutions in SPT in eqs. (4.1) and (4.5):

$$\begin{aligned}
P_{1\text{-loop}}(k)|_{\text{high-}k} &= P_{13,\text{high-}k}(k) + P_{22,\text{high-}k}(k) = 0, \\
P_{2\text{-loop}}(k)|_{\text{high-}k} &= P_{33a,\text{high-}k}(k) + P_{33b,\text{high-}k}(k) + P_{24,\text{high-}k}(k) + P_{15,\text{high-}k}(k) = 0. \tag{4.8}
\end{aligned}$$

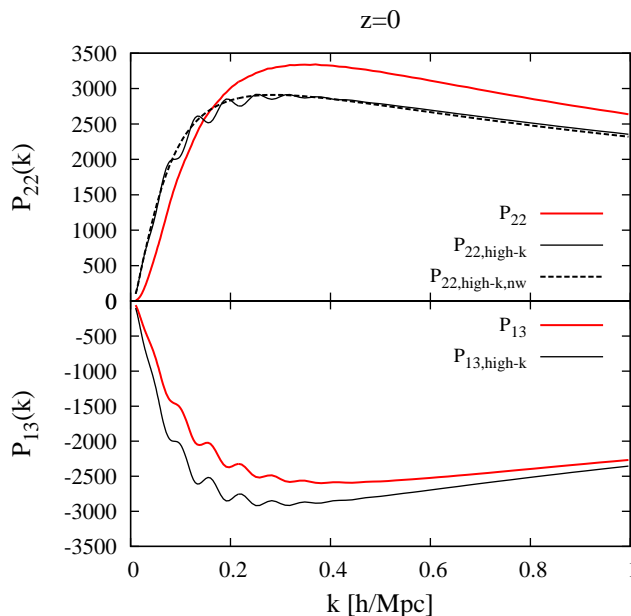


Figure 1. The exact solutions of P_{22} and P_{13} [eq. (A.2)] and the high- k solutions without the short-wavelength modes $P_{22,\text{high-}k}$ and $P_{13,\text{high-}k}$ [eq. (4.1)] are plotted as the red and black solid lines, respectively. The black dashed line denotes the no-wiggle high- k solution for P_{22} [eq. (C.1)].

Figures 1 and 2 show that the high- k solutions have considerable contributions in each solution of SPT even at low- k , though they completely cancel out each other. Thus, the cancellation of the high- k solutions in SPT is very important to accurately compute the non-linear power spectrum even at low- k , and we can understand their origin from the decomposition of the matter density perturbation into the short- and long-wavelength parts.

Here, we define the following quantities which satisfy the cancellation at the high- k limit:

$$\begin{aligned} P_{22}^{(S)}(k) &\equiv P_{22}(k) - P_{22,\text{high-}k}(k), \\ P_{13}^{(S)}(k) &\equiv P_{13}(k) - P_{13,\text{high-}k}(k), \end{aligned} \quad (4.9)$$

and

$$\begin{aligned} P_{33a}^{(S)}(k) &\equiv P_{33a}(k) - P_{33a,\text{high-}k}(k), \\ P_{33b}^{(S)}(k) &\equiv P_{33b}(k) - P_{33b,\text{high-}k}(k), \\ P_{24}^{(S)}(k) &\equiv P_{24}(k) - P_{24,\text{high-}k}(k), \\ P_{15}^{(S)}(k) &\equiv P_{15}(k) - P_{15,\text{high-}k}(k). \end{aligned} \quad (4.10)$$

These quantities yield from the correlation between the long-wavelength displacement vector $\bar{\Psi}^{(L)}$ and the short-wavelength matter density perturbation $\delta^{(S)}$. In this paper, we call these quantities the short-wavelength parts of the power spectrum. Then, the 1- and 2-loop solutions in SPT are

$$\begin{aligned} P_{1\text{-loop}}(k) &= P_{13}(k) + P_{22}(k) = P_{13}^{(S)}(k) + P_{22}^{(S)}(k) = P_{1\text{-loop}}^{(S)}(k), \\ P_{2\text{-loop}}(k) &= P_{33a}(k) + P_{33b}(k) + P_{24}(k) + P_{15}(k) = P_{33a}^{(S)}(k) + P_{33b}^{(S)}(k) + P_{24}^{(S)}(k) + P_{15}^{(S)}(k) = P_{2\text{-loop}}^{(S)}(k). \end{aligned} \quad (4.11)$$

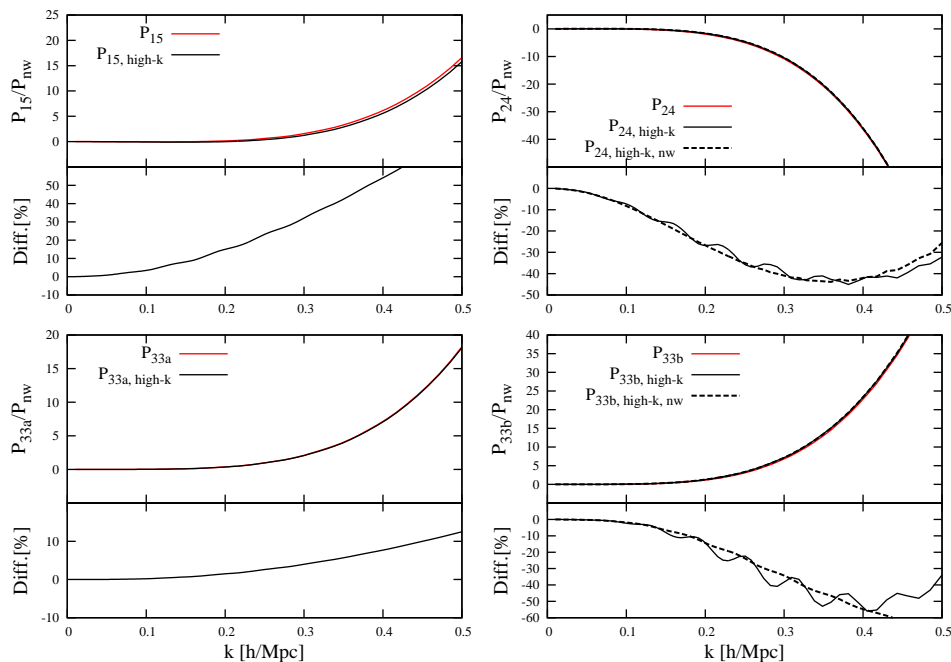


Figure 2. The exact solutions for P_{15} , P_{24} , P_{33a} and P_{33b} [eq. (A.3)], their high- k solutions [eq. (4.5)], and the no-wiggle high- k solutions for P_{24} and P_{33b} [eq. (C.3)] are plotted as the red solid, black solid, and black dashed lines, respectively. The fractional differences defined as $\text{Diff.}[\%] \equiv (P_{\text{exact}} - P_{\text{high-k}}) * 100 / P_{\text{lin}}^{\text{nw}}$ are also plotted as the black solid lines, where the no-wiggle linear power spectrum $P_{\text{lin}}^{\text{nw}}$ is presented in [48]. For P_{24} and P_{33b} , the fractional differences between the exact solutions and the no-wiggle high- k solutions are plotted as the black dashed lines.

The relation between between the original power spectrum and the short-wavelength power spectrum $P^{(S)}$, such as eqs. (4.9) and (4.10), are generalized as follows

$$P(z, k) = \exp\left(-\frac{\Sigma_v^2(z, k)}{2}\right) \exp\left(\frac{\Sigma_v^2(z, k)}{2}\right) \left[D^2 P_{\text{lin}}(k) + \sum_{n=1}^{\infty} D^{2n+2} P_{\text{n-loop}}^{(S)}(k) \right] = P^{(S)}(z, k) \quad (4.12)$$

where Σ_v^2 is defined as

$$\frac{\Sigma_v^2(z, k)}{2} \equiv 2 \sum_{n=1}^{\infty} \frac{(-1)^{n-1}}{(2n)!} \left\langle \left[\mathbf{k} \cdot \bar{\Psi}^{(L)}(z) \right]^{2n} \right\rangle_c, \quad (4.13)$$

and $\langle \dots \rangle_c$ denotes the cumulant. The definition of $\Sigma_v^2/2$ coincides with eq. (9) in [20]. At the 1-loop order, Σ_v^2 is proportional to k^2 and becomes

$$\Sigma_v^2(z, k) \equiv k^2 \bar{\Sigma}_v^2(z) = k^2 D^2 \sigma_{v,\text{lin}}^2 + k^2 D^4 \sigma_{v,1\text{-loop}}^2. \quad (4.14)$$

4.2 Comparison with previous works

4.2.1 RegPT

Before we proceed, we shall briefly review the multi-point propagator method (Γ -expansion method) [27, 28, 32, 34]. In the Γ -expansion method, the full non-linear power spectrum is described as

$$P(z, k) = \sum_{r=1}^{\infty} P_{\Gamma}^{(r)}(z, k), \quad (4.15)$$

where $P_\Gamma^{(r)}$ is the r th-order contribution to the power spectrum in the Γ -expansion, defined as

$$P_\Gamma^{(r)}(z, k) \equiv r! \int \frac{d^3 k_1}{(2\pi)^3} \cdots \int \frac{d^3 k_r}{(2\pi)^3} (2\pi)^3 \delta_D(\mathbf{k} - \mathbf{k}_{[1,r]}) \left[\Gamma^{(r)}(z, [\mathbf{k}_1, \mathbf{k}_r]) \right]^2 P_{\text{lin}}(k_1) \cdots P_{\text{lin}}(k_r). \quad (4.16)$$

The relation between the coefficient of the Γ -expansion and the kernel function in SPT is given by

$$\Gamma^{(r)}(z, [\mathbf{k}_1, \mathbf{k}_r]) \equiv D^r \Gamma_{\text{tree}}^{(r)}([\mathbf{k}_1, \mathbf{k}_r]) + \sum_{n=1}^{\infty} D^{r+2n} \Gamma_{\text{n-loop}}^{(r)}([\mathbf{k}_1, \mathbf{k}_r]), \quad (4.17)$$

where

$$\begin{aligned} \Gamma_{\text{tree}}^{(r)}([\mathbf{k}_1, \mathbf{k}_r]) &\equiv F_r([\mathbf{k}_1, \mathbf{k}_r]), \\ \Gamma_{\text{n-loop}}^{(r)}([\mathbf{k}_1, \mathbf{k}_r]) &\equiv \frac{1}{r!} \frac{(r+2n)!}{2^n n!} \int \frac{d^3 p_1}{(2\pi)^3} \cdots \int \frac{d^3 p_n}{(2\pi)^3} F_{r+2n}([\mathbf{k}_1, \mathbf{k}_r], \mathbf{p}_1, -\mathbf{p}_1, \dots, \mathbf{p}_n, -\mathbf{p}_n) P_{\text{lin}}(p_1) \cdots P_{\text{lin}}(p_n). \end{aligned} \quad (4.18)$$

At the 2-loop order in SPT, the loop correction terms are classified by the Γ -expansion as

$$\begin{aligned} P_\Gamma^{(1)}(z, k) &= \left[\Gamma^{(1)}(z, k) \right]^2 P_{\text{lin}}(k) = D^2 P_{\text{lin}}(k) + D^4 P_{13}(k) + D^6 P_{33a}(k) + D^6 P_{15}(k), \\ P_\Gamma^{(2)}(z, k) &= D^4 P_{22}(k) + D^6 P_{24}(k), \\ P_\Gamma^{(3)}(z, k) &= D^6 P_{33b}(k). \end{aligned} \quad (4.19)$$

Note that $\Gamma^{(1)}$ is defined as

$$\langle \delta(z, \mathbf{k}) \delta_{\text{lin}}(z=0, \mathbf{k}') \rangle \equiv (2\pi)^3 \delta_D(\mathbf{k} + \mathbf{k}') \Gamma^{(1)}(z, k) P_{\text{lin}}(k), \quad (4.20)$$

and called the ‘‘propagator’’ in RPT [22–24] and RegPT [27, 28, 32, 33].

In our previous work [18], we gave an alternative explanation for RegPT and proposed its extended version [eq. (40) in [18]] using the expression of the kernel functions in eq. (2.4). Here, we review RegPT in our context focusing the cancellation of the high- k solutions in SPT. For this purpose, we truncate the short-wavelength correction terms in eq. (4.12) as follows

$$\begin{aligned} P(z, k) &= \exp\left(-\frac{k^2 D^2 \sigma_{\text{v,lin}}^2}{2}\right) \sum_{n=0}^{\infty} \frac{1}{n!} \left(\frac{k^2 D^2 \sigma_{\text{v,lin}}^2}{2}\right)^n \\ &\times \left[D^2 P_{\text{lin}}(k) + D^4 \left(P_{22}^{(S)}(k) + P_{13}^{(S)}(k) \right) + D^6 \left(P_{33a}^{(S)}(k) + P_{33b}^{(S)}(k) + P_{24}^{(S)}(k) + P_{15}^{(S)}(k) \right) \right. \\ &\quad \left. + D^8 \left(P_{44a}^{(S)}(k) + \frac{P_{13}^{(S)}(k) P_{15}^{(S)}(k)}{2 P_{\text{lin}}(k)} \right) + D^{10} \frac{\left[P_{15}^{(S)}(k) \right]^2}{4 P_{\text{lin}}(k)} \right], \end{aligned} \quad (4.21)$$

where we ignored the 1-loop velocity dispersion $\bar{\Sigma}_{\text{v}}^2(z) = D^2 \sigma_{\text{v,lin}}^2$ and considered the exact 1- and 2-loop corrections as well as the partial 3-loop and 4-loop corrections for the short-wavelength terms: namely $D^4 P_{1\text{-loop}}$, $D^6 P_{2\text{-loop}}$, $D^8 \left(P_{44a}^{(S)} + P_{13}^{(S)} P_{15}^{(S)} / (2 P_{\text{lin}}) \right)$, and $D^{10} (P_{15}^{(S)})^2 / (4 P_{\text{lin}})$, respectively.

$P_{44a}^{(S)}$ [eq. (A.4)], which satisfies the cancellation at the high- k limit, is given by

$$P_{44a}(k) = P_{44a}^{(S)}(k) - \frac{1}{2} \left(\frac{k^2 \sigma_{\text{v,lin}}^2}{2} \right) P_{24}(k) - \frac{1}{4} \left(\frac{k^2 \sigma_{\text{v,lin}}^2}{2} \right)^2 P_{22}(k) + \left(\frac{k^2 \sigma_{\text{v,lin}}^2}{2} \right) \left[\frac{P_{13}(k)}{2 P_{\text{lin}}(k)} + \frac{k^2 \sigma_{\text{v,lin}}^2}{4} \right]^2 P_{\text{lin}}(k). \quad (4.22)$$

Then, we can rewrite eq. (4.21) as

$$\begin{aligned}
P(z, k) &= \sum_{r=1}^{\infty} P_{\Gamma}^{(r)}(z, k) \\
&= \exp\left(-\frac{k^2 D^2 \sigma_{v,\text{lin}}^2}{2}\right) \sum_{r=1}^{\infty} \frac{1}{(r-1)!} \left(\frac{k^2 D^2 \sigma_{v,\text{lin}}^2}{2}\right)^{r-1} D^2 P_{\text{lin}}(k) \left[1 + D^2 \frac{P_{13}^{(S)}(k)}{2P_{\text{lin}}(k)} + D^4 \frac{P_{15}^{(S)}(k)}{2P_{\text{lin}}(k)}\right]^2 \\
&\quad + \exp\left(-\frac{k^2 D^2 \sigma_{v,\text{lin}}^2}{2}\right) \sum_{r=2}^{\infty} \frac{1}{(r-2)!} \left(\frac{k^2 D^2 \sigma_{v,\text{lin}}^2}{2}\right)^{r-2} \left[D^4 P_{22}^{(S)}(k) + D^6 P_{24}^{(S)}(k) + D^8 P_{44a}^{(S)}(k)\right] \\
&\quad + \exp\left(-\frac{k^2 D^2 \sigma_{v,\text{lin}}^2}{2}\right) \sum_{r=3}^{\infty} \frac{1}{(r-3)!} \left(\frac{k^2 D^2 \sigma_{v,\text{lin}}^2}{2}\right)^{r-3} \left[D^6 P_{33b}^{(S)}(k)\right], \tag{4.23}
\end{aligned}$$

This expression coincides with the result of the extended Reg PT [eq. (40) in [18]]. The integer r corresponds to the order of the Γ -expansion. When we truncate the order of the Γ -expansion at the third order, we reproduce the original Reg PT solution at the 2-loop order (for details, see [18]). Equations (4.21) and (4.23) lead to

$$P(z, k) = D^2 P_{\text{lin}}(k) + D^4 P_{1\text{-loop}}(k) + D^6 P_{2\text{-loop}} + D^8 \left(P_{44a}^{(S)}(k) + \frac{P_{13}^{(S)}(k) P_{15}^{(S)}(k)}{2P_{\text{lin}}(k)} \right) + D^{10} \frac{[P_{15}^{(S)}(k)]^2}{4P_{\text{lin}}(k)}. \tag{4.24}$$

This expression is coincident with eq. (43) in [18].

Our previous work [18] pointed out that the RegPT solution behaves as a part of the SPT solution and its predicted power spectrum amplitude tend to be smaller than SPT (see figure 2 in [18]). Now, we can understand this reason. In RegPT, the higher loop correction terms than the 2-loop order in SPT which satisfy the cancellation at the high- k limit are only three terms: $D^4 P_{1\text{-loop}}$, $D^6 P_{2\text{-loop}}$, $D^8 \left(P_{44a}^{(S)} + P_{13}^{(S)} P_{15}^{(S)} / (2P_{\text{lin}}) \right)$, and $D^{10} (P_{15}^{(S)})^2 / (4P_{\text{lin}})$. However, their correction terms hardly contribute to the power spectrum at large scales (see figure 1 in [18]). On the other hand, at small scales where they can not be ignored, the exponential damping factor becomes dominant. Therefore, the amplitude of the solution in RegPT always tends to be smaller than that in SPT.

The propagator is useful for analyzing BAO, described by summing up all terms proportional to the linear power spectrum:

$$\begin{aligned}
\langle \delta(z, \mathbf{k}) \delta_{\text{lin}}(z=0, \mathbf{k}') \rangle &= (2\pi)^3 \delta_{\text{D}}(\mathbf{k} + \mathbf{k}') \left[1 + \sum_{n=1}^{\infty} D^{2n} \frac{P_{1(2n+1)}(k)}{2P_{\text{lin}}(k)} \right] D P_{\text{lin}}(k) \\
&= (2\pi)^3 \delta_{\text{D}}(\mathbf{k} + \mathbf{k}') \exp\left(-\frac{\Sigma_{\text{v}}^2(z, k)}{4}\right) \left[1 + \sum_{n=1}^{\infty} D^{2n} \frac{P_{1(2n+1)}^{(S)}(k)}{2P_{\text{lin}}(k)} \right] D P_{\text{lin}}(k), \tag{4.25}
\end{aligned}$$

Thus, we obtain the exponential damping behavior in the propagator by defining the short-wavelength term. In other words, the above relation is the definition of $P_{1(2n+1)}^{(S)}$. This exponential damping behavior of the propagator is well known (for example, see [47]). Actually, when we truncate the long- and short-wavelength contributions up to the 2-loop level, we have the similar expression to eq. (43) in [47].

$$\Gamma^{(1)}(z, k) = \exp\left(-\frac{k^2 D^2 \sigma_{v,\text{lin}}^2 + k^2 D^4 \sigma_{v,1\text{-loop}}^2}{4}\right) \left[1 + D^2 \frac{P_{13}^{(S)}(k)}{2P_{\text{lin}}(k)} + D^4 \frac{P_{15}^{(S)}(k)}{2P_{\text{lin}}(k)} \right] D. \tag{4.26}$$

Again, note that our definition of the 1-loop velocity dispersion [eq. (4.6)] is different from eq. (41) in [47].

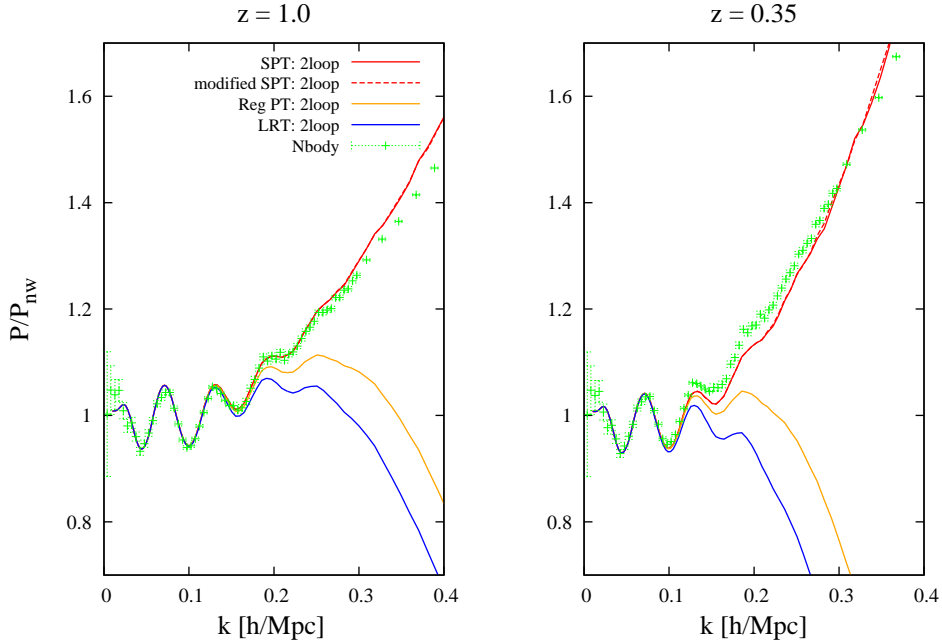


Figure 3. The theoretical predictions at the 2-loop level (SPT [eq. (4.11)], modified SPT [eq. (5.2)], Reg PT [eq. (4.23)], LRT [eq. (4.28)]) and the N -body simulation results are plotted as the red solid, red dashed, orange solid, blue solid lines, and the green symbols at $z = 1.0$ and $z = 0.35$.

4.2.2 Comparison with LRT

The original LRT was proposed as a theory to describe perturbative regime before shell-crossing, and as mentioned in [cite], LRT was not designed for the high- k regime where exponential damping factor is important. Similarly to RegPT, LRT has non-linear correction terms that do not guarantee the cancellation of the high- k solutions in SPT. In particular, their terms that correspond to 3- and more loop orders in SPT do not satisfy the cancellation. The regime where LRT is applicable is the low- k regime where this cancellation is not important.

Equation (4.12) coincides with the generalized formalism of LRT (see eq. (2.5) in [21]):

$$\begin{aligned}
 P(z, k) &= \exp\left(-\frac{\Sigma_v^2(z, k)}{2}\right) \exp\left(\frac{\Sigma_v^2(z, k)}{2}\right) \left[D^2 P_{\text{lin}}(k) + \sum_{n=1}^{\infty} D^{2n+2} P_{n\text{-loop}}^{(S)}(k) \right] \\
 &= \exp\left(-\frac{\Sigma_v^2(z, k)}{2}\right) \exp\left(\frac{\Sigma_v^2(z, k)}{2}\right) \left[D^2 P_{\text{lin}}(k) + \sum_{n=1}^{\infty} D^{2n+2} P_{n\text{-loop}}(k) \right], \quad (4.27)
 \end{aligned}$$

where we used $P_{n\text{-loop}} = P_{n\text{-loop}}^{(S)}$.

To derive the LRT solution with the 2-loop corrections, we truncate the short-wavelength correction terms at the 2-loop level and the velocity dispersion at the 1-loop level, and partially expand

the exponential factor $\exp(k^2\bar{\Sigma}_v^2/2)$ in eq. (4.27) as follows:

$$\begin{aligned}
P_{\text{LRT},2\text{loop}}(z, k) = & \exp\left(-\frac{k^2 D^2 \sigma_{v,\text{lin}}^2 + k^2 D^4 \sigma_{v,1\text{-loop}}^2}{2}\right) \left[D^2 P_{\text{lin}}(k) + D^4 P_{1\text{-loop}}(k) + D^6 P_{2\text{-loop}}(k) \right. \\
& + \left(1 + \frac{k^2 D^2 \sigma_{v,\text{lin}}^2 + k^2 D^4 \sigma_{v,1\text{-loop}}^2}{2} + \frac{1}{2!} \left(\frac{k^2 D^2 \sigma_{v,\text{lin}}^2}{2} \right)^2 \right) D^2 P_{\text{lin}}(k) \\
& \left. + \left(1 + \frac{k^2 D^2 \sigma_{v,\text{lin}}^2}{2} \right) D^4 P_{1\text{-loop}}(k) \right]. \tag{4.28}
\end{aligned}$$

As shown in figure 3, RegPT and LRT tend to predict the power spectrum amplitudes that are smaller than SPT (see also figure 2 in [18]) because of their exponential damping behavior.

5 Accurate BAO behavior in the power spectrum

So far, we have showed that we need to consider the short-wavelength modes to get the accurate information on the non-linear evolution of dark matter, but not the global coordinate transformation effect from the long-wavelength displacement vector. However, it is impossible to exactly compute higher order corrections of the short-wavelength modes. In this section we propose a model for calculating the non-linear power spectrum including the non-linear shift of BAO in higher order short-wavelength terms than the 2-loop level.

To this end, let us emphasize that the first coefficient of the Γ -expansion $P_\Gamma^{(1)} = [\Gamma^{(1)}]^2 P_{\text{lin}}$ includes the oscillation behavior due to the linear power spectrum, while by definition the other terms $P_\Gamma^{(r)}$ ($r \geq 2$) have no oscillatory behavior because they are computed from the integration of the linear power spectrum and their oscillation behavior in the linear power spectrum is smoothed [eq. (4.15)] (also see eq. (9) in [24]). Furthermore, based on the Γ -expansion the full non-linear power spectrum is generally represented as follows:

$$P(z, k) = [\Gamma^{(1)}(z, k)]^2 P_{\text{lin}}^{\text{nw}}(k) + \sum_{n=2}^{\infty} P_\Gamma^{(n)}(z, k) + [\Gamma^{(1)}(z, k)]^2 [P_{\text{lin}}(k) - P_{\text{lin}}^{\text{nw}}(k)], \tag{5.1}$$

where the no-wiggle linear power spectrum $P_{\text{lin}}^{\text{nw}}$ is presented in [48]. This expression is exact and intuitive. While the first and second terms represent the amplitude of the non-linear power spectrum without the oscillation behavior, the third term only contains the non-linear evolution of BAO.

Remind that we have derived the correction terms in the Γ -expansion in eq. (4.23) for all orders. However, $P_\Gamma^{(n)}$ ($n \geq 2$) as calculated in eq. (4.23) has the oscillatory behavior due to the linear power spectrum. This is because we have truncated the short-wavelength mode at a finite order (the 2-loop level plus some extra terms). Thus, the lack of the information on higher than 2-loop order short-wavelength terms causes the incorrect BAO behavior in the power spectrum.

Therefore, we propose a simple prescription to modify the incorrect BAO behavior. We just replace the linear power spectrum in $P_\Gamma^{(n)}$ ($n \geq 2$) calculated in eq. (4.23) with the no-wiggle linear power spectrum (see also appendix C). Through this replacement, we can get more accurate oscillation behavior in the power spectrum, even though the amplitude of the power spectrum is not corrected. Eventually, we get the following expression:

$$\begin{aligned}
P(z, k) = & D^2 P_{\text{lin}}^{\text{nw}}(k) + D^4 P_{1\text{-loop}}^{\text{nw}}(k) + D^6 P_{2\text{-loop}}^{\text{nw}}(k) \\
& + \exp\left(-\frac{k^2 \bar{\Sigma}_v^2(z)}{2}\right) \left[1 + D^2 \frac{P_{13}^{(S)}(k)}{2P_{\text{lin}}(k)} + D^4 \frac{P_{15}^{(S)}(k)}{2P_{\text{lin}}(k)} \right]^2 D^2 [P_{\text{lin}}(k) - P_{\text{lin}}^{\text{nw}}(k)], \tag{5.2}
\end{aligned}$$

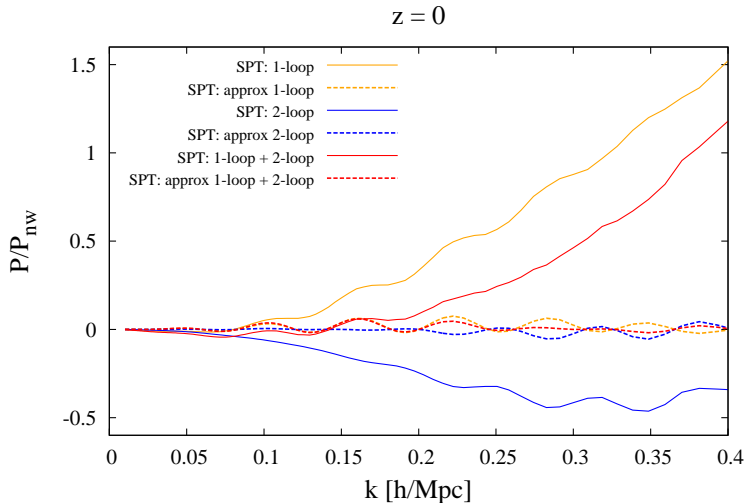


Figure 4. The exact and approximated 1- and 2-loop correction terms $P_{1\text{-loop}}$, $P_{2\text{-loop}}$, and $P_{1\text{-loop}} + P_{2\text{-loop}}$ are plotted as the orange, blue, and red solid (dashed) lines.

where the no-wiggle 1- and 2-loop corrections are defined as

$$\begin{aligned}
 P_{1\text{-loop}}^{\text{nw}}(k) &\equiv \frac{P_{\text{lin}}^{\text{nw}}(k)}{P_{\text{lin}}(k)} P_{13}(k) + P_{22}(k), \\
 P_{2\text{-loop}}^{\text{nw}}(k) &\equiv \frac{P_{\text{lin}}^{\text{nw}}(k)}{P_{\text{lin}}(k)} [P_{33a}(k) + P_{15}(k)] + P_{24}(k) + P_{33b}(k),
 \end{aligned}
 \tag{5.3}$$

and we considered the non-linear velocity dispersion at up to the 1-loop level: $\bar{\Sigma}_{\text{v}}^2(z) = D^2 \sigma_{\text{v,lin}}^2 + D^4 \sigma_{\text{v,1-loop}}^2$ as given in eq. (4.14). This is the second main result of this paper. The first line in eq. (5.2) corresponds to the first and second terms in eq. (5.1) which represent the amplitude of the power spectrum without the BAO behavior. On the other hand, the second line term in eq. (5.2) corresponds to the third term in eq. (5.1) which only has the non-linear BAO behavior with its amplitude centered around zero. Note that implicitly in the front of the first line in eq. (5.2) there is the translational symmetry factor $\exp(-k^2 \bar{\Sigma}_{\text{v}}^2/2) \exp(k^2 \bar{\Sigma}_{\text{v}}^2/2) = 1$. When we expand the exponential factor $\exp(-k^2 \bar{\Sigma}_{\text{v}}^2/2)$ in the second line, we get the usual SPT 2-loop solution as well as higher order correction terms. Thus, this model has the more effective information of BAO than the usual SPT 2-loop solution, and approximately includes higher loop short-wavelength modes than the 2-loop level: $P_{n\text{-loop}}^{(S)}$ ($n \geq 3$). However, as shown in figure 3, our modified SPT solution [eq. (5.2)] is hardly different from the usual SPT 2-loop solution at BAO scales. This means that the additional correction terms to the BAO behavior beyond the SPT 2-loop solution [eq. (5.2)] are small enough to be ignored at least at $z = 1.0$ and $z = 0.35$.

To test the validity of the above expression [eq. (5.2)], we apply to the same approximation used

in the derivation of eq. (5.2) to the linear power spectrum:

$$\begin{aligned}
P(z, k) &= \exp\left(-\frac{k^2 \bar{\Sigma}_v^2(z)}{2}\right) \exp\left(\frac{k^2 \bar{\Sigma}_v^2(z)}{2}\right) D^2 P_{\text{lin}}(k) \\
&= \exp\left(-\frac{k^2 \bar{\Sigma}_v^2(z)}{2}\right) D^2 P_{\text{lin}}(k) + \exp\left(-\frac{k^2 \bar{\Sigma}_v^2(z)}{2}\right) \left(\exp\left(\frac{k^2 \bar{\Sigma}_v^2(z)}{2}\right) - 1\right) D^2 P_{\text{lin}}(k) \\
&\rightarrow \exp\left(-\frac{k^2 \bar{\Sigma}_v^2(z)}{2}\right) D^2 P_{\text{lin}}(k) + \exp\left(-\frac{k^2 \bar{\Sigma}_v^2(z)}{2}\right) \left(\exp\left(\frac{k^2 \bar{\Sigma}_v^2(z)}{2}\right) - 1\right) D^2 P_{\text{lin}}^{\text{nw}}(k) \\
&= D^2 P_{\text{lin}}^{\text{nw}}(k) + \exp\left(-\frac{k^2 \bar{\Sigma}_v^2(z)}{2}\right) D^2 (P_{\text{lin}}(k) - P_{\text{lin}}^{\text{nw}}(k)), \tag{5.4}
\end{aligned}$$

where in the third line we replaced the linear power spectrum of the second term with the no-wiggle linear power spectrum. This model has no correction to the amplitude of the power spectrum and its amplitude is almost the same as the linear power spectrum. However, this model includes the correction terms to the BAO behavior. From eq. (5.4), the approximated 1- and 2-loop correction terms are described as (see also appendix C)

$$\begin{aligned}
P_{1\text{-loop}}(k) &\rightarrow -\left(\frac{k^2 \sigma_{v,\text{lin}}^2}{2}\right) (P_{\text{lin}}(k) - P_{\text{lin}}^{\text{nw}}(k)), \\
P_{2\text{-loop}}(k) &\rightarrow \left(\frac{1}{2} \left(\frac{k^2 \sigma_{v,\text{lin}}^2}{2}\right)^2 - \left(\frac{k^2 \sigma_{v,1\text{-loop}}^2}{2}\right)\right) (P_{\text{lin}}(k) - P_{\text{lin}}^{\text{nw}}(k)). \tag{5.5}
\end{aligned}$$

In figure 4, we find that the exact solutions of $P_{1\text{-loop}}$ and $P_{2\text{-loop}}$ have a different phase of BAO and tend to cancel out each other, yielding the somewhat smoothed correction term [red solid line in figure 4]. On the other hand, the approximated 1- and 2-loop solutions [eq. (5.5)] explain this cancellation of the oscillation behavior [red dashed line in figure 4], even though their amplitudes are centered around zero. Thus, the modified linear power spectrum indeed has effective corrections to the non-linear BAO behavior. This fact guarantees that our result [eq. (5.2)] includes higher order corrections than the 2-loop level and corrects the non-linear evolution of BAO compared to the usual SPT 2-loop solution [eq. (4.11)].

In figure 5, we compare the various predictions for the non-linear evolution of BAO: linear, 1-loop, 2-loop, the modified linear model [eq. (5.4)], and our new result [eq. 5.2]. The linear, 1-loop, and 2-loop BAO behaviors are defined as

$$\begin{aligned}
P_{\text{BAO,lin}}(z, k) &\equiv D^2 (P_{\text{lin}}(k) - P_{\text{lin}}^{\text{nw}}(k)), \\
P_{\text{BAO,1-loop}}(z, k) &\equiv D^2 (P_{\text{lin}}(k) - P_{\text{lin}}^{\text{nw}}(k)) + D^4 (P_{1\text{-loop}}(k) - P_{1\text{-loop}}^{\text{nw}}(k)) \\
&= P_{\text{BAO,lin}}(z, k) + D^4 (P_{13}(k) - P_{13}^{\text{nw}}(k)), \\
P_{\text{BAO,2-loop}}(z, k) &\equiv D^2 (P_{\text{lin}}(k) - P_{\text{lin}}^{\text{nw}}(k)) + D^4 (P_{1\text{-loop}}(k) - P_{1\text{-loop}}^{\text{nw}}(k)) + D^6 (P_{2\text{-loop}}(k) - P_{2\text{-loop}}^{\text{nw}}(k)) \\
&= P_{\text{BAO,1-loop}}(z, k) + D^6 (P_{15}(k) - P_{15}^{\text{nw}}(k) + P_{33a}(k) - P_{33a}^{\text{nw}}(k)). \tag{5.6}
\end{aligned}$$

At $z = 0$ [right panel in figure 5], we find that the SPT 1- and 2-loop solutions have the different BAO behavior from our result, especially at high- k . In particular, the SPT 1-loop solution has a different phase of BAO. At $z = 2.0$, these differences are suppressed.

Let us consider the physical meaning of our result [eq. (5.2)]. The exponential factor $\exp(-k^2 \bar{\Sigma}_v^2(z)/2)$ in eq. (5.2) comes from the large-scale velocity field (the long-wavelength displacement vector $\bar{\Psi}^{(L)}$). This factor causes the acoustic feature to be broader, reducing the amplitude of the acoustic oscillation (see blue line in figure 5). On the other hand, the factor

$$\left[1 + D^2 \frac{P_{13}^{(S)}(k)}{2P_{\text{lin}}(k)} + D^4 \frac{P_{15}^{(S)}(k)}{2P_{\text{lin}}(k)}\right]^2 \tag{5.7}$$

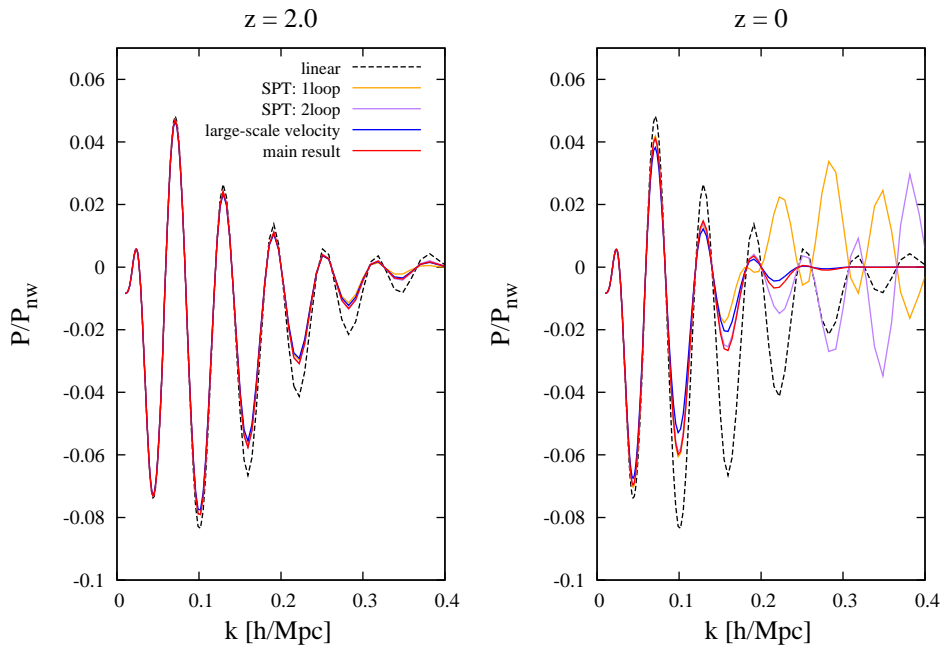


Figure 5. The various predictions of the evolution of BAO are plotted. The linear, 1-loop, and 2-loop corrections to BAO given in eq. (5.6) are plotted as the black dashed, orange solid, purple solid lines. The BAO behavior in the modified linear model (the second term in eq. (5.4)) and our result (the second line in eq. (5.2)) are plotted by the blue and red solid lines, respectively.

is caused by the gravitational effect between dark matter particles. The gravitational effect restricts the movement of dark matter particles, preventing the acoustic feature to be spread out by the large-scale velocity of dark matter. As a result, the reduced amplitude of the BAO peak by the large-scale velocity slightly increases (see red line in figure 5).

One might wonder why our model [eq. (5.2)] has the exponential damping factor computed by the long-wavelength displacement vector. This is because of the short-wavelength matter perturbations, but not due to the global coordinate transformation. The long-wavelength displacement vector can affect the matter power spectrum through the short-wavelength matter perturbation.

We conclude this section by discussing the smoothed linear power spectrum without the BAO feature. Although the no-wiggle linear power spectrum $P_{\text{lin}}^{\text{nw}}$ presented in [48] has been widely used, its amplitude does not exactly coincide with the linear power spectrum, especially in the high- k region. Therefore, our model [eq. (5.2)] largely differs from the usual SPT 2-loop solution [eq. (4.11)] at small scales. However, as long as we only focus on BAO scales ($k \leq 0.4h/\text{Mpc}$), the difference is not important, at least at $z = 0.35$ [figure 3].

6 Correlation function

Usually, it is not possible to compute the correlation function in models based on SPT because of the divergence of the solutions at high- k (see figure. 4). However, truncating the Γ -expansion (the LRT expansion) at a finite order leads to exponentially suppressed power spectrum and enables a computation of the correlation function. In this paper, we also adopt this prescription. Simply, we

use the following expression:

$$\begin{aligned}
P(z, k) = & \exp\left(-\frac{k^2 \bar{\Sigma}_v^2(z)}{2}\right) \sum_{n=0}^6 \frac{1}{n!} \left(\frac{k^2 \bar{\Sigma}_v^2(z)}{2}\right)^n [D^2 P_{\text{lin}}^{\text{nw}}(k) + D^4 P_{1\text{-loop}}^{\text{nw}}(k) + D^6 P_{2\text{-loop}}^{\text{nw}}(k)] \\
& + \exp\left(-\frac{k^2 \bar{\Sigma}_v^2(z)}{2}\right) \left[1 + D^2 \frac{P_{13}^{(S)}(k)}{2P_{\text{lin}}(k)} + D^4 \frac{P_{15}^{(S)}(k)}{2P_{\text{lin}}(k)}\right]^2 [D^2 P_{\text{lin}}(k) - D^2 P_{\text{lin}}^{\text{nw}}(k)]. \quad (6.1)
\end{aligned}$$

In the right panel of figure 6, the correlation functions computed by the above model indeed reproduce the N -body simulations at $z = 1.0$ and 0.5 . There, we plot $r^2 \xi(r)$ which is proportional to the number of excess pairs in an annulus of width dr centered at r .

To clarify the physical meaning of the non-linear shift of BAO, we also plot the smoothed correlation functions without BAO and the BAO peak functions, defined as (see the left panel in figure 6)

$$\begin{aligned}
\xi_{\text{lin}}(z, r) &= \xi_{\text{lin}}^{\text{nw}}(z, r) + \xi_{\text{lin}}^{\text{BAO}}(z, r), \\
\xi_v(z, r) &= \xi_{\text{lin}}^{\text{nw}}(z, r) + \xi_v^{\text{BAO}}(z, r), \\
\xi_{\text{nl}}(z, r) &= \xi_{\text{nl}}^{\text{nw}}(z, r) + \xi_{\text{nl}}^{\text{BAO}}(z, r),
\end{aligned} \quad (6.2)$$

where

$$\begin{aligned}
\xi_{\text{lin}}^{\text{nw}}(z, r) &\equiv \int \frac{dk}{2\pi^2} k^2 j_0(kr) D^2 P_{\text{lin}}^{\text{nw}}(k), \\
\xi_{\text{nl}}^{\text{nw}}(z, r) &\equiv \int \frac{dk}{2\pi^2} k^2 j_0(kr) \exp\left(-\frac{k^2 \bar{\Sigma}_v^2(z)}{2}\right) \sum_{n=0}^6 \frac{1}{n!} \left(\frac{k^2 \bar{\Sigma}_v^2(z)}{2}\right)^n [D^2 P_{\text{lin}}^{\text{nw}}(k) + D^4 P_{1\text{-loop}}^{\text{nw}}(k) + D^6 P_{2\text{-loop}}^{\text{nw}}(k)],
\end{aligned} \quad (6.3)$$

and

$$\begin{aligned}
\xi_{\text{lin}}^{\text{BAO}}(z, r) &\equiv \int \frac{dk}{2\pi^2} k^2 j_0(kr) D^2 [P_{\text{lin}}(k) - P_{\text{lin}}^{\text{nw}}(k)], \\
\xi_v^{\text{BAO}}(z, r) &\equiv \int \frac{dk}{2\pi^2} k^2 j_0(kr) \exp\left(-\frac{k^2 \bar{\Sigma}_v^2(z)}{2}\right) D^2 [P_{\text{lin}}(k) - P_{\text{lin}}^{\text{nw}}(k)] \\
&= \int_0^\infty ds I(z, r, s) \xi_{\text{lin}}^{\text{BAO}}(z, s), \\
\xi_{\text{nl}}^{\text{BAO}}(z, r) &\equiv \int \frac{dk}{2\pi^2} k^2 j_0(kr) \exp\left(-\frac{k^2 \bar{\Sigma}_v^2(z)}{2}\right) \left[1 + D^2 \frac{P_{13}^{(S)}(k)}{2P_{\text{lin}}(k)} + D^4 \frac{P_{15}^{(S)}(k)}{2P_{\text{lin}}(k)}\right]^2 D^2 [P_{\text{lin}}(k) - P_{\text{lin}}^{\text{nw}}(k)],
\end{aligned} \quad (6.4)$$

where $j_0(x) \equiv \sin(x)/x$, and the function I is

$$I(z, r, s) \equiv \frac{1}{\sqrt{2\pi \bar{\Sigma}_v^2(z)}} \frac{s}{r} \left\{ \exp\left[-\frac{(s-r)^2}{2\bar{\Sigma}_v^2(z)}\right] - \exp\left[-\frac{(s+r)^2}{2\bar{\Sigma}_v^2(z)}\right] \right\} \quad (6.5)$$

and satisfies $\int_0^\infty ds I(z, r, s) = 1$.

From eqs. (6.3), we find that the non-linear evolution of the amplitude of the matter perturbation hardly affects the correlation function around the BAO peak even at $z = 0$ (see the red and black dashed lines in figure 6). This is because the scales around the BAO peak are too large to neglect the non-linear evolution of the amplitude of the matter perturbation. On the other hand, the dominant contribution to the non-linear shift of BAO comes from ξ^{BAO} in eqs. (6.4), which is computed by the second line in eq. (5.2) and the second term in eq. (5.4). As we expected and showed in the case of the

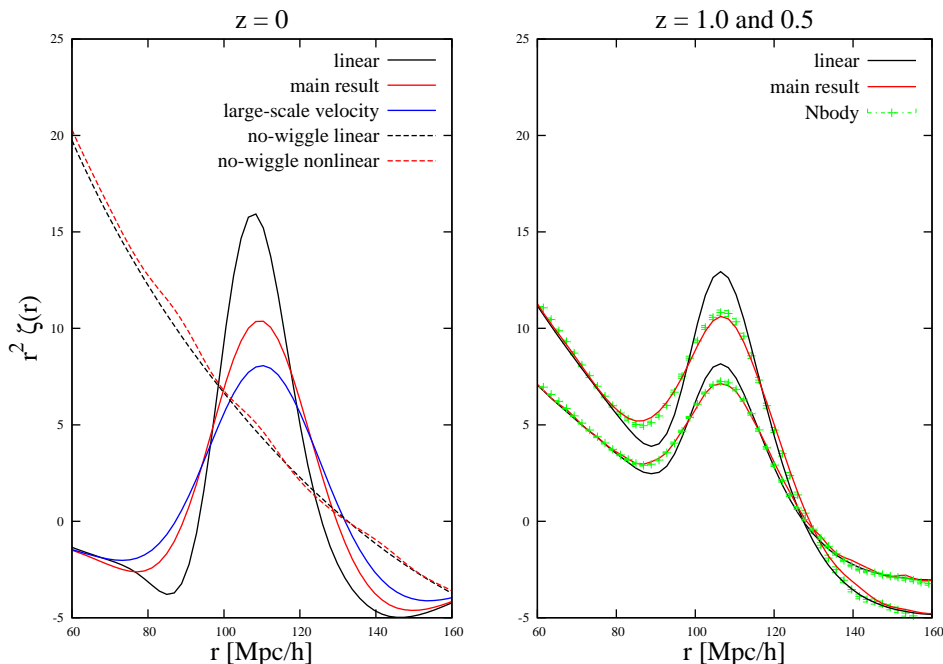


Figure 6. In the left panel, the smoothed correlation functions without the BAO peak $r^2 \xi_{\text{lin}}^{\text{nw}}$ and $r^2 \xi_{\text{nl}}^{\text{nw}}$ defined in eqs. (6.3) and the BAO peak functions $r^2 \xi_{\text{lin}}^{\text{BAO}}$, $r^2 \xi_{\text{v}}^{\text{BAO}}$, and $r^2 \xi_{\text{nl}}^{\text{BAO}}$ are plotted by the black dashed, red dashed, black solid, blue solid, and red solid lines, respectively at $z = 0$. In the right panel, the predicted correlation functions computed by the linear power spectrum and our model [eq. (6.1)], and the N -body simulations are plotted by the black solid lines, red solid lines, and green symbols at $z = 1.0$ and 0.5 .

power spectrum, while the large-scale velocity field (the factor $\exp(-k^2 \bar{\Sigma}_v^2/2)$) causes the BAO peak to be broader, the gravitational effect between dark matter particles (the factor in eq. (5.7)) prevents the movement of dark matter particles, slightly increasing the spread BAO peak (see the blue and red solid lines in the left panel of figure 6). Thus, the gravitational effect between dark matter particles is a non-negligible effect when predicting the non-linear correlation function.

We want to mention that the modified linear model [eq. (5.4)] we presented has the same form as the template model to construct the fitting formula of the non-linear power spectrum in [49–53]². The authors in [51] fixed the smoothing parameter as $\bar{\Sigma}_v = 8 \text{ Mpc}/h$ before the reconstruction at $z = 0.35$. Now, we can predict the value of $\bar{\Sigma}_v$ from eq. (4.14). Figure 7 shows the predicted smoothing parameters in the range of $5.0 \leq z \leq 0$. At $z = 0.35$, we have $\bar{\Sigma}_v(z = 0.35) = 7.2 \text{ Mpc}/h$ and $\bar{\Sigma}_v(z = 0.35) = 7.7 \text{ Mpc}/h$ at the linear and 1-loop level, respectively. Thus, we have the correct smoothing parameter by including the 1-loop level velocity dispersion $\sigma_{1\text{-loop}}$. Furthermore, using our model [eq. (5.2)] we could improve the fitting formula of the non-linear power spectrum in [51]. This work is left for a future study.

6.1 BAO peak shift

We consider the shift of the BAO peak position caused by the non-linear evolution. In Figure 8, we showed the BAO peak positions of ξ_{lin} (black solid line), $\xi_{\text{lin}}^{\text{BAO}}$ (black dashed line), $\xi_{\text{v}}^{\text{BAO}}$ (red dashed line), $\xi_{\text{nl}}^{\text{BAO}}$ (red dashed line), and ξ_{nl} (red solid line) in the range of redshifts $5.0 \leq z \leq 0$. Their peak positions are numerically computed by the Newton method.

² See eq. (14) in [51], where the smoothed linear power spectrum and the smoothing parameter are represented by P_{smooth} and Σ_{nl} .

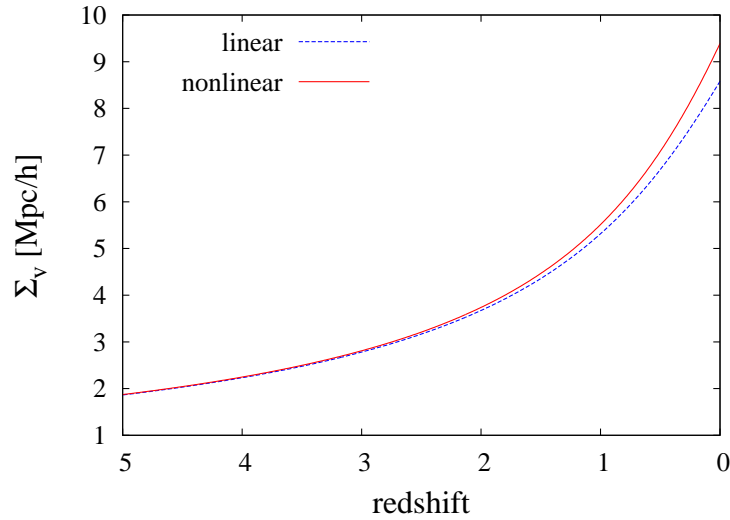


Figure 7. Smoothing parameters $\bar{\Sigma}_v$ at the linear and 1-loop level are plotted as the blue dashed and red solid lines, respectively, in the range of redshifts $5 \leq z \leq 0$.

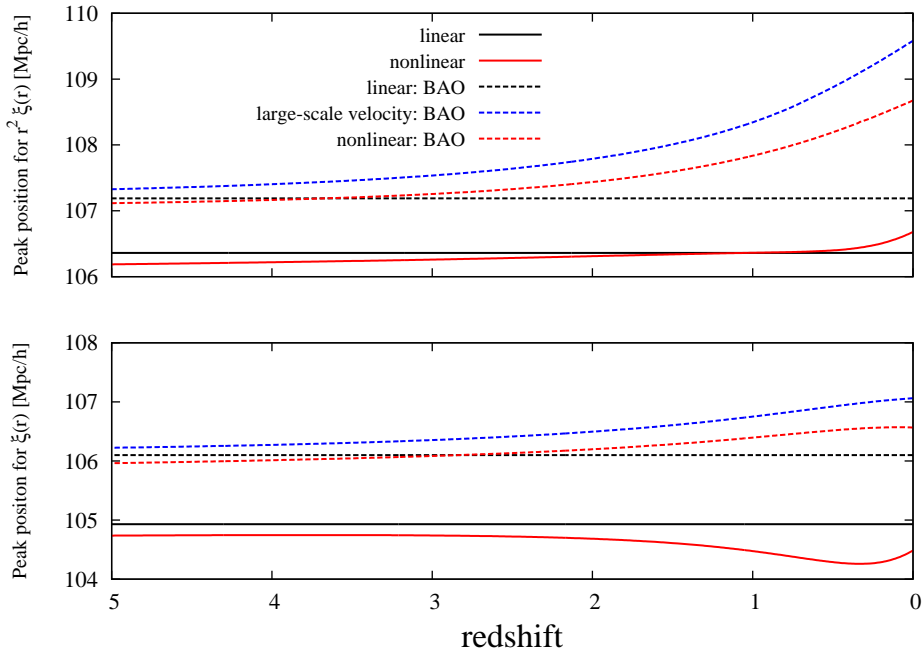


Figure 8. Top panel: BAO peak positions of $r^2 \xi_{\text{lin}}$, $r^2 \xi_{\text{lin}}^{\text{BAO}}$, $r^2 \xi_v^{\text{BAO}}$, $r^2 \xi_{\text{nl}}^{\text{BAO}}$, and $r^2 \xi_{\text{nl}}$ are plotted as the black solid, black dashed, blue dashed, red dashed, and red solid lines, respectively, in the range of redshifts $5.0 \leq z \leq 0$. Bottom panel: Same as the top panel, where the BAO peak positions of ξ_{lin} , $\xi_{\text{lin}}^{\text{BAO}}$, ξ_v^{BAO} , $\xi_{\text{nl}}^{\text{BAO}}$, and ξ_{nl} are plotted.

First, we focus on the linear correlation function $r^2 \xi_{\text{lin}}$ whose BAO peak is at ~ 106.4 Mpc/h. (see the black solid line in the top panel of Figure 8). By decomposing into the gravitational collapse effect $r^2 \xi_{\text{lin}}^{\text{nw}}$ and the BAO effect $r^2 \xi_{\text{lin}}^{\text{BAO}}$ (eq. (6.2)), the linear BAO peak function $r^2 \xi_{\text{lin}}^{\text{BAO}}$ has its

peak at $\sim 107.1 \text{ Mpc}/h$ (see the black solid line in the left panel of Figure 6 and the black dashed line in the top panel of Figure 8). In other words, the linear gravitational collapse shifts the linear BAO peak position of $r^2 \xi_{\text{lin}}^{\text{BAO}}$ to small scales. In the linear theory, this shift of the BAO peak does not depend on redshifts. Next, the large-scale velocity field effect shifts the BAO peak to large scales. This feature is expressed by the function I [eq. (6.5)] and ξ_v^{BAO} [eq. (6.4)] (see the blue line in the left panel of Figure 6 and the blue dashed line in the top panel of Figure 8). We can roughly estimate this BAO peak shift caused by the large-scale velocity field as follows. Since in the black line in the left panel of Figure 6 the function $r^2 \xi_{\text{lin}}^{\text{BAO}}$ is very peaked around its peak position $r_s \sim 107.1 \text{ Mpc}/h$, we assume that $r^2 \xi_{\text{lin}}^{\text{BAO}}$ is proportional to $\delta_D(r - r_s)$. Then, the spread BAO peak function by the large scale velocity field becomes

$$\begin{aligned} r^2 \xi_v^{\text{BAO}}(z, r) &\propto \frac{1}{\sqrt{2\pi\bar{\Sigma}_v^2(z)}} \frac{r}{r_s} \left\{ \exp\left[-\frac{(r-r_s)^2}{2\bar{\Sigma}_v^2(z)}\right] - \exp\left[-\frac{(r+r_s)^2}{2\bar{\Sigma}_v^2(z)}\right] \right\}, \\ &\sim \frac{1}{\sqrt{2\pi\bar{\Sigma}_v^2(z)}} \frac{r}{r_s} \exp\left[-\frac{(r-r_s)^2}{2\bar{\Sigma}_v^2(z)}\right], \end{aligned} \quad (6.6)$$

where the second term in the first line is negligibly small when $r_s \gg 1$. By solving the following equation

$$\frac{\partial}{\partial r} (r^2 \xi_v^{\text{BAO}}(z, r)) = 0, \quad (6.7)$$

we have the shifted BAO peak position as

$$\begin{aligned} r_v^{\text{BAO}} &= \frac{r_s}{2} + \frac{\sqrt{r_s^2 + 4\bar{\Sigma}_v^2(z)}}{2}, \\ &\sim r_s + \frac{\bar{\Sigma}_v^2(z)}{r_s}, \end{aligned} \quad (6.8)$$

where we used $\bar{\Sigma}_v^2/r_s^2 \ll 1$. Thus, the change of the BAO peak position caused by the large-scale velocity field is estimated using the large-scale velocity dispersion $\bar{\Sigma}_v$ as $\bar{\Sigma}_v^2/r_s$. Third, the gravitational effect restrict the movement of dark matter particles, slightly increasing the height of the spread BAO peak by the large-scale velocity field and shifting the BAO peak position to small scales (see the red line in the left panel of Figure 6 and the red dashed line in the top panel of Figure 8). Finally, adding the non-linear gravitational collapse effect $\xi_{\text{nl}}^{\text{nw}}$ the BAO peak position further shifts to small scales (see the red solid line in the top panel of Figure 8). Because of the cancellation of the large-scale velocity field effect and the gravitational effect, the final value of the BAO peak shift becomes small and is less than $1 \text{ Mpc}/h$. Also for the correlation function ξ , the same analysis can be done (see the bottom panel in Figure 8).

7 Conclusion

We showed that it is possible to describe the matter perturbation as a global coordinate transformation from the long-wavelength displacement vector acting on the short-wavelength matter density perturbation. This feature allows to understand the well known cancellation of the SPT solution at the high- k limit. The high- k limit contributions in SPT are dominant in each correction term at the 1- and 2-loop orders, such as P_{13} , P_{22} , P_{33a} , P_{33b} , P_{24} , and P_{15} , even though their high- k solutions completely cancel out in the total correction terms at the 1- and 2-loop orders. Some of the recently proposed improved perturbation theories, such as RegPT and LRT, have correction terms which do not guarantee the cancellation in their expansion approach. Because of this, they both tend to predict the power spectrum amplitudes that are smaller than SPT. This implies that SPT still predicts the non-linear power spectrum accurately.

As an example of the model for going beyond SPT, we presented the model of the non-linear power spectrum which is based on the SPT 2-loop solution, but more accurately captures the effect of short-wavelength modes and large scale motions on the BAO peak position and shape. From

this model, we have the intuitive behavior of BAO in the correlation function. We showed that the non-linear evolution of the BAO peak in the correlation function mainly has two effects. First, the height of the BAO peak is spread by the large-scale velocity field (the long-wavelength displacement vector). Second, the gravitational effect restricts the movement of dark matter particles, slightly suppressing this spreading of the BAO peak. The non-linear evolution of the amplitude of the dark matter perturbation does not have a significant influence on the non-linear BAO evolution. Our model motivates the template model used to constrain the cosmological parameters from the BAO feature in [50–53], and correctly predicts the smoothing parameter by including the 1-loop velocity dispersion: $\bar{\Sigma}_v \sim 7.7 \text{ Mpc}/h$ at $z = 0.35$. Using our model we estimated the value of the BAO peak shift in Figure 8, and showed that the BAO peak shift is less than $1 \text{ Mpc}/h$ in the range of redshifts $5.0 \leq z \leq 0$. The reason why the BAO peak shift caused by the non-linear evolution is small is because of the cancellation between the large-scale velocity field effect and the gravitational effect. That is, while the large-scale velocity field shifts the BAO peak to large scales, the gravitational effect shifts it to small scales. Finally, we note that it might be useful for BAO peak analyses to use $r^2\xi - r^2\xi_{\text{lin}}^{\text{nw}}$ whose shift of the BAO peak is more visible than $r^2\xi$, where we do not need to consider the non-linear gravitational collapse $r^2\xi_{\text{nl}}^{\text{nw}}$ because around the BAO peak position the gravitational effect is well represented by the linear theory (see the black and red dashed lines in the left panel of Figure 6).

Acknowledgments

We thank T. Futamase, A. Taruya, T. Matsubara, E. Pajer, M. Zaldarriaga, and L. Mercoli for useful comments, and we thank to T. Nishimichi for providing the numerical simulation results. This work is supported by a Grant-in-Aid for Scientific Research from JSPS (No. 24-3849 for N.S.S.). N.S.S. thanks to Department of Astrophysical Science at Princeton University for providing a good environment for research.

A Definition of the 1- and 2-loop correction terms in SPT

The definitions of the 1- and 2-loop correction terms are given as follows:

$$\begin{aligned} P_{1\text{-loop}}(k) &\equiv P_{22}(k) + P_{13}(k), \\ P_{2\text{-loop}}(k) &\equiv P_{15}(k) + P_{24}(k) + P_{33a}(k) + P_{33b}(k), \end{aligned} \quad (\text{A.1})$$

where

$$\begin{aligned} P_{13}(k) &\equiv 6P_{\text{lin}}(k) \int \frac{d^3p}{(2\pi)^3} F_3(\mathbf{k}, \mathbf{p}, -\mathbf{p}) P_{\text{lin}}(p), \\ P_{22}(k) &\equiv 2 \int \frac{d^3k_1}{(2\pi)^3} \frac{d^3k_2}{(2\pi)^3} (2\pi)^3 \delta_D(\mathbf{k} - \mathbf{k}_{[1,2]}) [F_2(\mathbf{k}_1, \mathbf{k}_2)]^2 P_{\text{lin}}(k_1) P_{\text{lin}}(k_2), \end{aligned} \quad (\text{A.2})$$

and

$$\begin{aligned} P_{15}(k) &\equiv 30P_{\text{lin}}(k) \int \frac{d^3p_1}{(2\pi)^3} \frac{d^3p_2}{(2\pi)^3} F_5(\mathbf{k}, \mathbf{p}_1, -\mathbf{p}_1, \mathbf{p}_2, -\mathbf{p}_2) P_{\text{lin}}(p_1) P_{\text{lin}}(p_2), \\ P_{33a}(k) &\equiv \frac{(P_{13}(k))^2}{4P_{\text{lin}}(k)}, \\ P_{24}(k) &\equiv 24 \int \frac{d^3k_1}{(2\pi)^3} \frac{d^3k_2}{(2\pi)^3} \frac{d^3p}{(2\pi)^3} (2\pi)^3 \delta_D(\mathbf{k} - \mathbf{k}_{[1,2]}) F_2(\mathbf{k}_1, \mathbf{k}_2) F_4(\mathbf{k}_1, \mathbf{k}_2, \mathbf{p}, -\mathbf{p}) P_{\text{lin}}(p) P_{\text{lin}}(k_1) P_{\text{lin}}(k_2), \\ P_{33b}(k) &\equiv 6 \int \frac{d^3k_1}{(2\pi)^3} \frac{d^3k_2}{(2\pi)^3} \frac{d^3k_3}{(2\pi)^3} (2\pi)^3 \delta_D(\mathbf{k} - \mathbf{k}_{[1,3]}) [F_3(\mathbf{k}_1, \mathbf{k}_2, \mathbf{k}_3)]^2 P_{\text{lin}}(k_1) P_{\text{lin}}(k_2) P_{\text{lin}}(k_3). \end{aligned} \quad (\text{A.3})$$

Furthermore, a partial correction term at the 3-loop level in SPT P_{44a} is defined as

$$\begin{aligned} P_{44a}(k) &\equiv 72 \int \frac{d^3k_1}{(2\pi)^3} \frac{d^3k_2}{(2\pi)^3} \frac{d^3p_1}{(2\pi)^3} \frac{d^3p_2}{(2\pi)^3} (2\pi)^3 \delta_D(\mathbf{k} - \mathbf{k}_{[1,2]}) \\ &\quad \times F_4(\mathbf{k}_1, \mathbf{k}_2, \mathbf{p}_1, -\mathbf{p}_1) F_4(\mathbf{k}_1, \mathbf{k}_2, \mathbf{p}_2, -\mathbf{p}_2) P_{\text{lin}}(k_1) P_{\text{lin}}(k_2) P_{\text{lin}}(p_1) P_{\text{lin}}(p_2). \end{aligned} \quad (\text{A.4})$$

B Kernel functions of the Lagrangian perturbation theory

We summarize the definition of the kernel function \mathbf{L} in the Lagrangian perturbation theory and the non-linear velocity dispersions $\sigma_{v,1\text{-loop}}^2$.

The displacement vector is described as

$$\Psi(z, \mathbf{k}) = i \sum_{n=1}^{\infty} \frac{D^n}{n!} \int \frac{d^3 p_1}{(2\pi)^3} \cdots \frac{d^3 p_n}{(2\pi)^3} (2\pi)^3 \delta_{\text{D}}(\mathbf{k} - \mathbf{p}_{[1,n]}) \mathbf{L}_n(\mathbf{p}_1, \dots, \mathbf{p}_n) \delta_{\text{lin}}(\mathbf{p}_1) \cdots \delta_{\text{lin}}(\mathbf{p}_n). \quad (\text{B.1})$$

Similarly, the very long-wavelength displacement vector $\bar{\Psi}^{(L)}(z)$ is expanded as

$$\bar{\Psi}^{(L)}(z) \equiv i \sum_{n=1}^{\infty} \frac{D^n}{n!} \int \frac{d^3 p_1}{(2\pi)^3} \cdots \frac{d^3 p_n}{(2\pi)^3} \mathbf{L}_n(\mathbf{p}_1, \dots, \mathbf{p}_n) \delta_{\text{lin}}(\mathbf{p}_1) \cdots \delta_{\text{lin}}(\mathbf{p}_n). \quad (\text{B.2})$$

The kernel functions at up to the third order are given by [54]

$$\begin{aligned} \mathbf{L}_1(\mathbf{p}) &= \frac{\mathbf{p}}{p^2}, \\ \mathbf{L}_2(\mathbf{p}_1, \mathbf{p}_2) &= \frac{3}{7} \frac{\mathbf{p}_{[1,2]}}{|\mathbf{p}_{[1,2]}|^2} \left(1 - \frac{(\mathbf{p}_1 \cdot \mathbf{p}_2)^2}{p_1^2 p_2^2} \right), \\ \mathbf{L}_3(\mathbf{p}_1, \mathbf{p}_2, \mathbf{p}_3) &= \left\{ \frac{5}{21} \frac{\mathbf{p}_{[1,3]}}{|\mathbf{p}_{[1,3]}|^2} \left(1 - \frac{(\mathbf{p}_1 \cdot \mathbf{p}_2)^2}{p_1^2 p_2^2} \right) \left(1 - \frac{(\mathbf{p}_3 \cdot (\mathbf{p}_1 + \mathbf{p}_2))^2}{p_3^2 |\mathbf{p}_1 + \mathbf{p}_2|^2} \right) + 2 \text{ perms.} \right\} \\ &\quad - \frac{1}{3} \frac{\mathbf{p}_{[1,3]}}{|\mathbf{p}_{[1,3]}|^2} \left(1 - \frac{(\mathbf{p}_1 \cdot \mathbf{p}_2)^2}{p_1^2 p_2^2} - \frac{(\mathbf{p}_1 \cdot \mathbf{p}_3)^2}{p_1^2 p_3^2} - \frac{(\mathbf{p}_2 \cdot \mathbf{p}_3)^2}{p_2^2 p_3^2} + 2 \frac{(\mathbf{p}_1 \cdot \mathbf{p}_2)(\mathbf{p}_2 \cdot \mathbf{p}_3)(\mathbf{p}_1 \cdot \mathbf{p}_3)}{p_1^2 p_2^2 p_3^2} \right) \\ &\quad + \left\{ \frac{1}{7} \frac{\mathbf{p}_{[1,2]}(\mathbf{p}_{[1,3]} \cdot \mathbf{p}_3) - \mathbf{p}_3(\mathbf{p}_{[1,3]} \cdot \mathbf{p}_{[1,2]})}{|\mathbf{p}_{[1,3]}|^2} \left(\frac{\mathbf{p}_3 \cdot \mathbf{p}_{[1,2]}}{p_3^2 |\mathbf{p}_{[1,2]}|^2} \right) \left(1 - \frac{(\mathbf{p}_1 \cdot \mathbf{p}_2)^2}{p_1^2 p_2^2} \right) + 2 \text{ perms} \right\}. \end{aligned} \quad (\text{B.3})$$

The non-linear velocity dispersions $\sigma_{v,22}^2$ and $\sigma_{v,13}^2$ are calculated as

$$\begin{aligned} k^2 \sigma_{v,22}^2 &\equiv - \int \frac{d^3 p_1}{(2\pi)^3} \int \frac{d^3 p_2}{(2\pi)^3} \mathbf{k} \cdot \mathbf{L}_2(\mathbf{p}_1, \mathbf{p}_2) \mathbf{k} \cdot \mathbf{L}_2(-\mathbf{p}_1, -\mathbf{p}_2) P_{\text{lin}}(p_1) P_{\text{lin}}(p_2) \\ &= \left(\frac{3}{7} \right)^2 \int \frac{d^3 p_1}{(2\pi)^3} \int \frac{d^3 p_2}{(2\pi)^3} \frac{(\mathbf{k} \cdot \mathbf{p}_{[1,2]})^2}{|\mathbf{p}_{[1,2]}|^4} \left(1 - \frac{(\mathbf{p}_1 \cdot \mathbf{p}_2)^2}{p_1^2 p_2^2} \right)^2 P_{\text{lin}}(p_1) P_{\text{lin}}(p_2) \\ &= \frac{1}{3} \left(\frac{3}{7} \right)^2 \int \frac{d^3 p_1}{(2\pi)^3} \int \frac{d^3 p_2}{(2\pi)^3} \frac{k^2}{|\mathbf{p}_{[1,2]}|^2} \left(1 - \frac{(\mathbf{p}_1 \cdot \mathbf{p}_2)^2}{p_1^2 p_2^2} \right)^2 P_{\text{lin}}(p_1) P_{\text{lin}}(p_2) \\ &= \frac{3k^2}{392 \cdot 32\pi^4} \int \frac{dp_1}{p_1^3} \frac{dp_2}{p_2^3} K(p_1, p_2) P_{\text{lin}}(p_1) P_{\text{lin}}(p_2), \end{aligned} \quad (\text{B.4})$$

$$\begin{aligned} k^2 \sigma_{v,13}^2 &\equiv -2 \int \frac{d^3 p_1}{(2\pi)^3} \int \frac{d^3 p_2}{(2\pi)^3} \mathbf{k} \cdot \mathbf{L}_1(\mathbf{p}_1) \mathbf{k} \cdot \mathbf{L}_3(-\mathbf{p}_1, \mathbf{p}_2, -\mathbf{p}_2) P_{\text{lin}}(p_1) P_{\text{lin}}(p_2) \\ &= \frac{10}{63} \int \frac{d^3 p_1}{(2\pi)^3} \int \frac{d^3 p_2}{(2\pi)^3} \frac{k^2}{p_1^2} \left(1 - \frac{(\mathbf{p}_1 \cdot \mathbf{p}_2)^2}{p_1^2 p_2^2} \right) \left(\frac{p_1^2 p_2^2 - (\mathbf{p}_1 \cdot \mathbf{p}_2)^2}{|\mathbf{p}_1 - \mathbf{p}_2|^2 p_2^2} + \frac{p_1^2 p_2^2 - (\mathbf{p}_1 \cdot \mathbf{p}_2)^2}{|\mathbf{p}_1 + \mathbf{p}_2|^2 p_2^2} \right) P_{\text{lin}}(p_1) P_{\text{lin}}(p_2) \\ &= \frac{20}{63} \int \frac{d^3 p_1}{(2\pi)^3} \int \frac{d^3 p_2}{(2\pi)^3} \frac{k^2}{|\mathbf{p}_1 + \mathbf{p}_2|^2} \left(1 - \frac{(\mathbf{p}_1 \cdot \mathbf{p}_2)^2}{p_1^2 p_2^2} \right)^2 P_{\text{lin}}(p_1) P_{\text{lin}}(p_2) \\ &= \frac{5k^2}{126 \cdot 32\pi^4} \int \frac{dp_1}{p_1^3} \frac{dp_2}{p_2^3} K(p_1, p_2) P_{\text{lin}}(p_1) P_{\text{lin}}(p_2), \end{aligned} \quad (\text{B.5})$$

where

$$K(p_1, p_2) = (p_1^2 - p_2^2)^4 \ln \left(\frac{(p_1 + p_2)^2}{(p_1 - p_2)^2} \right) - \frac{4}{3} p_1 p_2 (3p_1^6 - 11p_2^2 p_1^4 - 11p_1^2 p_2^4 + 3p_2^6). \quad (\text{B.6})$$

The 1-loop velocity dispersion is given by $\sigma_{\text{v},1\text{-loop}}^2 \equiv \sigma_{\text{v},22}^2 + \sigma_{\text{v},13}^2$.

C Smoothed high- k solutions

As shown in eq. (4.1), the high- k solution for P_{22} has the BAO behavior owing to the linear power spectrum. However, the exact solution for P_{22} does not have the oscillation behavior because it is computed by integrating the linear power spectrum. To modify this incorrect BAO behavior for P_{22} , we simply replace the linear power spectrum in the high- k solution for P_{22} with the no-wiggle linear power spectrum as follows:

$$P_{22}(k) \rightarrow \left(\frac{k^2 \sigma_{\text{v},\text{lin}}^2}{2} \right) P_{\text{lin}}^{\text{nw}}(k). \quad (\text{C.1})$$

This solution indeed behaves as the approximated solution of the exact P_{22} at least than the high- k solution for P_{22} (see figure 2), and give the following approximated 1-loop solution

$$P_{1\text{-loop}}(k) \rightarrow - \left(\frac{k^2 \sigma_{\text{v},\text{lin}}^2}{2} \right) (P_{\text{lin}}(k) - P_{\text{lin}}^{\text{nw}}(k)). \quad (\text{C.2})$$

Similarly, we have the following no-wiggle high- k solution for P_{33b} and P_{24} ,

$$\begin{aligned} P_{33b}(k) &\rightarrow \left(\frac{k^2 \sigma_{\text{v},\text{lin}}^2}{2} \right) P_{22}(k) - \frac{1}{2} \left(\frac{k^2 \sigma_{\text{v},\text{lin}}^2}{2} \right)^2 P_{\text{lin}}^{\text{nw}}(k) + \left(\frac{k^2 \sigma_{\text{v},22}^2}{2} \right) P_{\text{lin}}^{\text{nw}}(k), \\ P_{24}(k) &\rightarrow - \left(\frac{k^2 \sigma_{\text{v},\text{lin}}^2}{2} \right) P_{22}(k), \end{aligned} \quad (\text{C.3})$$

and these modified solutions have a more reasonable behavior as the approximation of the exact P_{24} and P_{33b} than the high- k solutions (see figure 2). When we use $P_{22} \rightarrow k^2 \sigma_{\text{v},\text{lin}}^2 P_{\text{lin}}^{\text{nw}}/2$ and $P_{13} \rightarrow -k^2 \sigma_{\text{v},\text{lin}}^2 P_{\text{lin}}/2$, we have

$$\begin{aligned} P_{33b}(k) &\rightarrow \frac{1}{2} \left(\frac{k^2 \sigma_{\text{v},\text{lin}}^2}{2} \right)^2 P_{\text{lin}}^{\text{nw}}(k) + \left(\frac{k^2 \sigma_{\text{v},22}^2}{2} \right) P_{\text{lin}}^{\text{nw}}(k), \\ P_{24}(k) &\rightarrow - \left(\frac{k^2 \sigma_{\text{v},\text{lin}}^2}{2} \right)^2 P_{\text{lin}}^{\text{nw}}(k) + \left(\frac{k^2 \sigma_{\text{v},13}^2}{2} \right) P_{\text{lin}}^{\text{nw}}(k). \end{aligned} \quad (\text{C.4})$$

Thus, these smoothed high- k solutions and the high- k solutions for P_{15} and P_{33a} give the approximated 2-loop solution as follows:

$$P_{2\text{-loop}}(k) \rightarrow \left(\frac{1}{2} \left(\frac{k^2 \sigma_{\text{v},\text{lin}}^2}{2} \right)^2 - \left(\frac{k^2 \sigma_{\text{v},1\text{-loop}}^2}{2} \right) \right) (P_{\text{lin}}(k) - P_{\text{lin}}^{\text{nw}}(k)). \quad (\text{C.5})$$

References

- [1] **SDSS Collaboration** Collaboration, D. J. Eisenstein *et. al.*, *Detection of the baryon acoustic peak in the large-scale correlation function of SDSS luminous red galaxies*, *Astrophys.J.* **633** (2005) 560–574, [[astro-ph/0501171](#)].

- [2] **2dFGRS Collaboration** Collaboration, S. Cole *et. al.*, *The 2dF Galaxy Redshift Survey: Power-spectrum analysis of the final dataset and cosmological implications*, *Mon.Not.Roy.Astron.Soc.* **362** (2005) 505–534, [[astro-ph/0501174](#)].
- [3] **SDSS Collaboration** Collaboration, M. Tegmark *et. al.*, *Cosmological Constraints from the SDSS Luminous Red Galaxies*, *Phys.Rev.* **D74** (2006) 123507, [[astro-ph/0608632](#)].
- [4] W. J. Percival, R. C. Nichol, D. J. Eisenstein, D. H. Weinberg, M. Fukugita, *et. al.*, *Measuring the matter density using baryon oscillations in the SDSS*, *Astrophys.J.* **657** (2007) 51–55, [[astro-ph/0608635](#)].
- [5] **SDSS Collaboration** Collaboration, W. J. Percival *et. al.*, *Baryon Acoustic Oscillations in the Sloan Digital Sky Survey Data Release 7 Galaxy Sample*, *Mon.Not.Roy.Astron.Soc.* **401** (2010) 2148–2168, [[arXiv:0907.1660](#)].
- [6] **SDSS Collaboration** Collaboration, E. A. Kazin *et. al.*, *The Baryonic Acoustic Feature and Large-Scale Clustering in the SDSS LRG Sample*, *Astrophys.J.* **710** (2010) 1444–1461, [[arXiv:0908.2598](#)].
- [7] F. Beutler, C. Blake, M. Colless, D. H. Jones, L. Staveley-Smith, *et. al.*, *The 6dF Galaxy Survey: Baryon Acoustic Oscillations and the Local Hubble Constant*, *Mon.Not.Roy.Astron.Soc.* **416** (2011) 3017–3032, [[arXiv:1106.3366](#)].
- [8] C. Blake, S. Brough, M. Colless, W. Couch, S. Croom, *et. al.*, *The WiggleZ Dark Energy Survey: the selection function and $z=0.6$ galaxy power spectrum*, *Mon.Not.Roy.Astron.Soc.* **406** (2010) 803–821, [[arXiv:1003.5721](#)].
- [9] C. Blake, K. Glazebrook, T. Davis, S. Brough, M. Colless, *et. al.*, *The WiggleZ Dark Energy Survey: measuring the cosmic expansion history using the Alcock-Paczynski test and distant supernovae*, *Mon.Not.Roy.Astron.Soc.* **418** (2011) 1725–1735, [[arXiv:1108.2637](#)].
- [10] C. Blake, E. Kazin, F. Beutler, T. Davis, D. Parkinson, *et. al.*, *The WiggleZ Dark Energy Survey: mapping the distance-redshift relation with baryon acoustic oscillations*, *Mon.Not.Roy.Astron.Soc.* **418** (2011) 1707–1724, [[arXiv:1108.2635](#)].
- [11] F. Bernardeau, S. Colombi, E. Gaztanaga, and R. Scoccimarro, *Large-scale structure of the universe and cosmological perturbation theory*, *Phys. Rept.* **367** (2002) 1–248, [[astro-ph/0112551](#)].
- [12] J. N. Fry, *The Galaxy correlation hierarchy in perturbation theory*, *Astrophys. J.* **279** (1984) 499–510.
- [13] M. H. Goroff, B. Grinstein, S. J. Rey, and M. B. Wise, *Coupling of Modes of Cosmological Mass Density Fluctuations*, *Astrophys. J.* **311** (1986) 6–14.
- [14] Y. Suto and M. Sasaki, *Quasi nonlinear theory of cosmological selfgravitating systems*, *Phys. Rev. Lett.* **66** (1991) 264–267.
- [15] N. Makino, M. Sasaki, and Y. Suto, *Analytic approach to the perturbative expansion of nonlinear gravitational fluctuations in cosmological density and velocity fields*, *Phys. Rev.* **D46** (1992) 585–602.
- [16] B. Jain and E. Bertschinger, *Second order power spectrum and nonlinear evolution at high redshift*, *Astrophys. J.* **431** (1994) 495, [[astro-ph/9311070](#)].
- [17] R. Scoccimarro and J. Frieman, *Loop Corrections in Non-Linear Cosmological Perturbation Theory II. Two-point Statistics and Self-Similarity*, *Astrophys. J.* **473** (1996) 620, [[astro-ph/9602070](#)].
- [18] N. S. Sugiyama and T. Futamase, *Relation between the Standard Perturbation Theory and Regularized Multi-point Propagator Method*, *Astrophys.J.* **769** (June, 2013) 106, [[arXiv:1303.2748](#)].
- [19] D. Jeong and E. Komatsu, *Perturbation theory reloaded: analytical calculation of non-linearity in baryonic oscillations in the real space matter power spectrum*, *Astrophys.J.* **651** (2006) 619–626, [[astro-ph/0604075](#)].
- [20] T. Matsubara, *Resumming Cosmological Perturbations via the Lagrangian Picture: One-loop Results in Real Space and in Redshift Space*, *Phys. Rev.* **D77** (2008) 063530, [[arXiv:0711.2521](#)].
- [21] T. Okamura, A. Taruya, and T. Matsubara, *Next-to-leading resummation of cosmological perturbations via the Lagrangian picture: 2-loop correction in real and redshift spaces*, *JCAP* **1108** (2011) 012, [[arXiv:1105.1491](#)].

- [22] M. Crocce and R. Scoccimarro, *Renormalized Cosmological Perturbation Theory*, *Phys. Rev.* **D73** (2006) 063519, [[astro-ph/0509418](#)].
- [23] M. Crocce and R. Scoccimarro, *Memory of Initial Conditions in Gravitational Clustering*, *Phys. Rev.* **D73** (2006) 063520, [[astro-ph/0509419](#)].
- [24] M. Crocce and R. Scoccimarro, *Nonlinear Evolution of Baryon Acoustic Oscillations*, *Phys. Rev.* **D77** (2008) 023533, [[arXiv:0704.2783](#)].
- [25] A. Taruya and T. Hiramatsu, *A Closure Theory for Nonlinear Evolution of Cosmological Power Spectra*, *Astrophys. J.* **674** (Feb., 2008) 617–635, [[arXiv:0708.1367](#)].
- [26] A. Taruya, T. Nishimichi, S. Saito, and T. Hiramatsu, *Nonlinear evolution of baryon acoustic oscillations from improved perturbation theory in real and redshift spaces*, *Phys. Rev.* **D80** (2009), no. 12 123503, [[arXiv:0906.0507](#)].
- [27] F. Bernardeau, M. Crocce, and R. Scoccimarro, *Multi-Point Propagators in Cosmological Gravitational Instability*, *Phys. Rev.* **D78** (2008) 103521, [[arXiv:0806.2334](#)].
- [28] F. Bernardeau, M. Crocce, and R. Scoccimarro, *Constructing Regularized Cosmic Propagators*, *Phys.Rev.* **D85** (2012) 123519, [[arXiv:1112.3895](#)].
- [29] D. Blas, M. Garny, and T. Konstandin, *On the non-linear scale of cosmological perturbation theory*, *JCAP* **1309** (2013) 024, [[arXiv:1304.1546](#)].
- [30] F. Bernardeau, N. Van de Rijdt, and F. Vernizzi, *Resummed propagators in multi-component cosmic fluids with the eikonal approximation*, *Phys.Rev.* **D85** (2012) 063509, [[arXiv:1109.3400](#)].
- [31] F. Bernardeau, N. Van de Rijdt, and F. Vernizzi, *Power spectra in the eikonal approximation with adiabatic and non-adiabatic modes*, [arXiv:1209.3662](#).
- [32] A. Taruya, F. Bernardeau, T. Nishimichi, and S. Codis, *RegPT: Direct and fast calculation of regularized cosmological power spectrum at two-loop order*, *Phys.Rev.* **D86** (2012) 103528, [[arXiv:1208.1191](#)].
- [33] A. Taruya, T. Nishimichi, and F. Bernardeau, *Precision modeling of redshift-space distortions from multi-point propagator expansion*, [arXiv:1301.3624](#).
- [34] N. S. Sugiyama and T. Futamase, *An Application of Wiener Hermite Expansion to Non-linear Evolution of Dark Matter*, *Astrophys.J.* **760** (2012) 114, [[arXiv:1210.1663](#)].
- [35] E. Pajer and M. Zaldarriaga, *On the Renormalization of the Effective Field Theory of Large Scale Structures*, [arXiv:1301.7182](#).
- [36] S. Tassev and M. Zaldarriaga, *Towards an Optimal Reconstruction of Baryon Oscillations*, *JCAP* **1210** (2012) 006, [[arXiv:1203.6066](#)].
- [37] P. Valageas, T. Nishimichi, and A. Taruya, *Matter power spectrum from a Lagrangian-space regularization of perturbation theory*, *Phys.Rev.* **D87** (2013) 083522, [[arXiv:1302.4533](#)].
- [38] H. Gil-Marín, C. Wagner, L. Verde, C. Porciani, and R. Jimenez, *Perturbation theory approach for the power spectrum: from dark matter in real space to haloes in redshift space*, *JCAP* **1211** (2012) 029, [[arXiv:1209.3771](#)].
- [39] X. Wang and A. Szalay, *Resummed Perturbation Theory of Galaxy Clustering*, *Phys.Rev.* **D86** (2012) 043508, [[arXiv:1204.0019](#)].
- [40] J. Carlson, B. Reid, and M. White, *Convolution Lagrangian perturbation theory for biased tracers*, [arXiv:1209.0780](#).
- [41] S. Tassev, M. Zaldarriaga, and D. Eisenstein, *Solving Large Scale Structure in Ten Easy Steps with COLA*, [arXiv:1301.0322](#).
- [42] C. Orban, *Keeping It Real: Revisiting a Real-Space Approach to Running Ensembles of Cosmological N-body Simulations*, *JCAP* **1305** (2013) 032, [[arXiv:1201.2082](#)].
- [43] P. Valageas and T. Nishimichi, *Combining perturbation theories with halo models*, *Astron.Astrophys.* **527** (2011) A87, [[arXiv:1009.0597](#)].
- [44] V. Springel, *The cosmological simulation code GADGET-2*, *Mon. Not. Roy. Astron. Soc.* **364** (2005)

1105–1134, [[astro-ph/0505010](#)].

- [45] M. Crocce, S. Pueblas, and R. Scoccimarro, *Transients from Initial Conditions in Cosmological Simulations*, *Mon. Not. Roy. Astron. Soc.* **373** (2006) 369–381, [[astro-ph/0606505](#)].
- [46] **WMAP** Collaboration, E. Komatsu *et. al.*, *Five-Year Wilkinson Microwave Anisotropy Probe (WMAP) *ataffilmark 1*) Observations:Cosmological Interpretation*, *Astrophys. J. Suppl.* **180** (2009) 330–376, [[arXiv:0803.0547](#)].
- [47] F. Bernardeau, A. Taruya, and T. Nishimichi, *Cosmic propagators at two-loop order*, [arXiv:1211.1571](#).
- [48] D. J. Eisenstein and W. Hu, *Baryonic Features in the Matter Transfer Function*, *Astrophys. J.* **496** (1998) 605, [[astro-ph/9709112](#)].
- [49] H.-J. Seo and D. J. Eisenstein, *Improved forecasts for the baryon acoustic oscillations and cosmological distance scale*, *Astrophys.J.* **665** (2007) 14–24, [[astro-ph/0701079](#)].
- [50] N. Padmanabhan, X. Xu, D. J. Eisenstein, R. Scalzo, A. J. Cuesta, *et. al.*, *A 2 per cent distance to $z=0.35$ by reconstructing baryon acoustic oscillations - I. Methods and application to the Sloan Digital Sky Survey*, *Mon.Not.Roy.Astron.Soc.* **427** (2012), no. 3 2132–2145, [[arXiv:1202.0090](#)].
- [51] X. Xu, N. Padmanabhan, D. J. Eisenstein, K. T. Mehta, and A. J. Cuesta, *A 2Fitting Techniques*, [arXiv:1202.0091](#).
- [52] K. T. Mehta, A. J. Cuesta, X. Xu, D. J. Eisenstein, and N. Padmanabhan, *A 2% Distance to $z = 0.35$ by Reconstructing Baryon Acoustic Oscillations - III : Cosmological Measurements and Interpretation*, [arXiv:1202.0092](#).
- [53] X. Xu, A. J. Cuesta, N. Padmanabhan, D. J. Eisenstein, and C. K. McBride, *Measuring D_A and H at $z=0.35$ from the SDSS DR7 LRGs using baryon acoustic oscillations*, [arXiv:1206.6732](#).
- [54] C. Rampf, *The recursion relation in Lagrangian perturbation theory*, *JCAP* **1212** (2012) 004, [[arXiv:1205.5274](#)].